AD NUMBER
ADA029716
LIMITATION CHANGES
TO: **Approved for public release; distribution is unlimited.**
FROM: **Distribution authorized to U.S. Gov't. agencies only; Test and Evaluation; AUG 1976. Other requests shall be referred to Ballistic Research Laboratories, Attn: DRXBR-TS, Aberdeen Proving Ground, MS 21005.**
AUTHORITY
BRL per DTIC Form 55

BRL R 1906

BRL

AD

REPORT NO. 1906

EVALUATION OF SIMPLE MODELS FOR THE ATTENUATION OF SHOCK WAVES BY VENTED PLATES

Fritz H. Oertel, Jr.

August 1976

USA BALLISTIC RESEARCH LABORATORIES
ABERDEEN PROVING GROUND, MARYLAND

Destroy this report when it is no longer needed.
Do not return it to the originator.

Secondary distribution of this report by originating or sponsoring activity is prohibited.

Additional copies of this report may be obtained from the National Technical Information Service, U.S. Department of Commerce, Springfield, Virginia 22151.

The findings in this report are not to be construed as an official Department of the Army position, unless so designated by other authorized documents.

UNCLASSIFIED

SECURITY CLASSIFICATION OF THIS PAGE (When Data Entered)

REPORT DOCUMENTATION PAGE

READ INSTRUCTIONS BEFORE COMPLETING FORM

1. REPORT NUMBER: BRL Report No. 1906	2. GOVT ACCESSION NO.
3. RECIPIENT'S CATALOG NUMBER	
4. TITLE (and Subtitle): EVALUATION OF SIMPLE MODELS FOR THE ATTENUATION OF SHOCK WAVES BY VENTED PLATES	5. TYPE OF REPORT & PERIOD COVERED: Final
	6. PERFORMING ORG. REPORT NUMBER
7. AUTHOR(s): Fritz H. Oertel, Jr.	8. CONTRACT OR GRANT NUMBER(s)
9. PERFORMING ORGANIZATION NAME AND ADDRESS: U.S. Army Ballistic Research Laboratories, Aberdeen Proving Ground, Maryland 21005	10. PROGRAM ELEMENT, PROJECT, TASK AREA & WORK UNIT NUMBERS: RDT&E 1W161102AH43
11. CONTROLLING OFFICE NAME AND ADDRESS: U.S. Army Materiel Development & Readiness Command, 5001 Eisenhower Avenue, Alexandria, Virginia 22333	12. REPORT DATE: AUGUST 1976
	13. NUMBER OF PAGES: 55
14. MONITORING AGENCY NAME & ADDRESS (if different from Controlling Office)	15. SECURITY CLASS. (of this report): UNCLASSIFIED
	15a. DECLASSIFICATION/DOWNGRADING SCHEDULE

16. DISTRIBUTION STATEMENT (of this Report)

Distribution limited to US Government agencies only; Test and Evaluation; August 1976. Other requests for this document must be referred to Director, USA Ballistic Research Laboratories, ATTN: DRXBR-TS, Aberdeen Proving Ground, Maryland 21005.

17. DISTRIBUTION STATEMENT (of the abstract entered in Block 20, if different from Report)

18. SUPPLEMENTARY NOTES

The work reported here was performed for, and funded by PA, A 4932 MM&T Project No. 5751264, Advanced Technology for Suppressive Shielding of Hazardous Production and Supply Operations for Production Base Modernization and Expansion Program.

19. KEY WORDS (Continue on reverse side if necessary and identify by block number)

Shock Waves	1-D Model
Suppressive Structures	Nozzle Flow
Vented Plates	Ideal Gas
Blast Attenuation	Inviscid Flow

20. ABSTRACT (Continue on reverse side if necessary and identify by block number) (ner)

In this report, the attenuation of shock waves upon passing through vented plates is analyzed using simple one-dimensional flow models. Inviscid, non-conducting ideal diatomic gas is assumed. Transmission of shock waves through single plates and through arrays of several plates in series is considered. Models are compared with each other and with experiment. One model is found to be easier to use and less time-consuming, and, simultaneously, agrees best with the experimental results over a wide range of conditions.

DD FORM 1 JAN 73 1473 EDITION OF 1 NOV 65 IS OBSOLETE

UNCLASSIFIED

SECURITY CLASSIFICATION OF THIS PAGE (When Data Entered)

TABLE OF CONTENTS

LIST OF ILLUSTRATIONS

LIST OF ILLUSTRATIONS

I. INTRODUCTION

Blast associated with an accidental explosion is a danger to personnel, structures, and equipment. One simple protective measure is to build a massive total-containment structure. However, in many cases some type of vented structure is called for, such as: structures with frangible or blow-out panels, or the types of vented structures described in reference 1.

In order to better understand the suppression of blast by vented structures, BRL is conducting suppression tests on scaled-down models of such structures[1]; and, in a 10.2cm diameter shock tube, tests are being conducted on panels of those structures--for which the vented area is not easy to determine--and on panels with holes drilled in them[2]--for which the vented area is well-known.

In this report, which is done in conjunction with the Applied Technology Program of the Suppressive Shielding Program, we compare the shock tube experiments done by the BRL[2] and others[3-5,7] for single-

---

1. *C. Kingery, R. Schumacher, and W. Ewing, "Internal Pressures from Explosions in Suppressive Structures," BRL IMR 403, Ballistic Research Laboratories, Aberdeen Proving Ground, MD., June 1975.* (Not Available)
2. *Private communication from Mr. C. Kingery, Ballistic Research Laboratories, Aberdeen Proving Ground, MD., November 1975.*
3. *L. Dresner and C. V. Chester, "Attenuation of Shocks in Tubes by Orifice Plates," ORNL - TM-1750, Oak Ridge National Laboratory, Oak Ridge, TN., 1967.*
4. *B. Anet, "Experimentelle Untersuchung über den Einfluss einer Einschnürung auf die Stosswellenausbreitung in einem Kanal Konstanter Querschnitts," Bericht SHB Nr. 68-17-G3, Studienkommission des EJPD für Zivilschutz, Zürich, Switzerland, 1968.*
5. *B. P. Bertrand, "Shock Wave Transmission through a Large Restriction in a Constant Area Duct," BRL MR 1848, Ballistic Research Laboratories, Aberdeen Proving Ground, MD., June 1967 (AD 656744).*
6. *L. L. Monroe, "Investigation of the Transmission of a Shock Wave through an Orifice," GALCIT Hypersonic Research Project Memorandum No. 46, Guggenheim Aeronautical Laboratory, California Institute of Technology, Pasadena, CA, September 1958.*
7. *J. M. Ross, C. M. Nixon, and W. M. McMurtry, "A Shock Tube Study of Attenuation of Air Flow through Chokes," Suffield Technical Note No. 152, Suffield Experimental Station, Ralston Alberta, Canada, May 1966.*

and multiple-plate arrays with the results of simple computation models[5-8].

II. PHYSICS OF THE INTERACTION

The interaction of a shock wave with a vented plate having a single venting slit is sketched in Figure 1, following a discussion in reference 4. In Figure 1a, the portion of the on-coming shock wave incident upon the obstruction is reflected by it, while the rest of the wave is transmitted into the hole undiminished in strength. After some time, the expansion wave shown propagating out from the opening serves to pump fluid into the hole and to attenuate the reflected shock wave.

The influence of viscosity is seen as a build-up of vortices at the entrance, Figure 1a. At a later time, this vortex becomes detached and is swept into the restriction, forming a contraction (*vena contracta*), Figures 1b-1e. Viscous effects are further in evidence as vortices are formed, Figure 1c, when the transmitted shock wave emerges from the restriction, later becoming detached, Figure 1e, as the shock wave expands to occupy the full area of the test section. For this particular case [incident shock strength: $\sim$ 18 psi (0.124 MPa)], an expansion wave propagates upstream against the flow, Figure 1c, causing an acceleration of the gas in the restriction until sonic flow is reached locally. It is noteworthy that sonic flow also exists at the smallest cross-section of the *vena contracta*, but a standing shock, Figures 1d and 1e, reestablishes subsonic flow.

Although the geometry of the vent in Figure 1 is not the same as for our cases, the concept should be equivalent. Some of the details of Figure 1 are supported by shadow photographs of shock waves interacting with thin plates vented by a single hole[7], by schlieren photographs of this interaction for various "slit" geometries[6], and by shadow[9,10] and interference[10] photographs of a shock wave leaving a tube.

---

8. *F. H. Oertel, N. Gerber, and J. M. Bartos, "The Modified Expansion Tube: Theory and Experiment," BRL R 1741, Ballistic Research Laboratories, Aberdeen Proving Ground, MD., September 1974, AD A001551.*

9. *E. M. Schmidt and D. D. Shear, "The Flow Field About an M-16 Rifle," BRL R 1692, Ballistic Research Laboratories, Aberdeen Proving Ground, MD., January 1974 (AD 916646L). Also "The Formation and Decay of Impulsive, Supersonic Jets," AIAA Paper No. 74-531, AIAA 7th Fluid and Plasma Dynamics Conference, Palo Alto, CA, June 1974.*

10. *F. H. Oertel, Jr., "Laser Interferometry of Unsteady, Underexpanded Jets," BRL R 1694, Ballistic Research Laboratories, Aberdeen Proving Ground, MD., January 1974 (AD 773664). Also Proc. Int'l. Cong. Instr. in Aerospace Simulation Facilities, CA Institute of Technology, Pasadena, CA, September 1973.*

In the case of a plate with several holes, the picture is conceptually the same for each hole. However, the interaction of the expansion waves at each hole with the reflected shock wave must be considered, as well as the interaction of the shock waves emanating from each hole. It is not known how long it takes for these shocks to form into a uniform front.

For more complex geometries, the flow is even more complex. As a consequence, care must be taken to ensure that gages are placed far enough from the structure for meaningful and consistent pressure measurements to be made. For example, even for the simple case in Figure 1, a gage placed several tube diameters from the plate would read the pressure jump across a quasi-one-dimensional shock wave (Figure 1e). A gage placed near the plate would not (see Figure 1d).

III. MODEL FORMULATION AND DISCUSSION OF SIMPLE MODELS - SINGLE VENTED PLATE

From the previous description, it is clear that the transmission of a pressure wave through a vented plate is highly complex, even for the case of the single vent opening in Figure 1. To make such a problem tractable, simplifying assumptions must be made. We have chosen to make a first order-type approximation, assuming that heat transfer, and local effects due to a sharp-edged restriction, such as: three-dimensionality, transiency, vorticity, flow separation, and turbulence, are of second order. The models shown in Figure 2 have been considered in this report.

In each model, we assume that for the incident and transmitted flows, steady, one-dimensional conservation equations for an inviscid, nonconducting, ideal diatomic gas are valid. For the transmitted shock wave, the flow is again steady and nearly one-dimensional far from the plate. And in each model, the assumptions made regarding the local flow through the vented plate reduce the complex flow through a sharp-edge restriction to the well-known case of steady, isentropic, quasi-one-dimensional flow through a convergent-divergent nozzle[11] -- as depicted in Figure 2. The nozzle has an area ratio A/A^*, where A is the unrestricted cross-sectional area of the tube and A^* is the sum of the cross-sectional areas of the holes. We assume that mass flow through the nozzle in each model is maximized; i.e., sonic or choked flow occurs at the throat, state [*].

Other aspects of the models are slightly different:

In Model 1, Figure 2a, which has been found to give good agreement with properties measured in the hypersonic flow downstream of

---

11. G. Rudinger, Nonsteady Duct Flow: Wave-Diagram Analysis, Dover Publications, Inc., New York, N. Y., 1969, p. 94.

the nozzle plate in the BRL expansion tube[12], the incident shock wave is assumed to be fully reflected from the plate so that $u_6 = 0$. An isentropic, unsteady expansion--similar to that for the instantaneous opening of a diaphragm--then accelerates the stagnated gas so that it enters the convergent nozzle with a velocity $u_{6'}$. During expansion in the nozzle from the state [*], the gas becomes underexpanded, requiring recompression. In this model, recompression is accomplished via unsteady, *isentropic compression*, the complementary process to the *isentropic expansion* needed in computing the expansion tube cycle. Of course, this process is not physically realistic. But, neither is the steady, isentropic nozzle expansion, which is merely an expedient of the one-dimensional simplified model that attempts to predict the end result of the actual unsteady free expansion from the constriction.

Model 2 is a composite used in reference 7 of Laporte's[13] model for flow into a constriction and Rudinger's[11] model for a shock wave diffracted by an increase in cross-section. Here, the incident shock wave is assumed to be partially reflected so that the gas flows into the nozzle with a velocity u_5. Conditions in region [5] are such that sonic flow will prevail at the nozzle throat. Then, the gas is accelerated by an unsteady, constant-area, isentropic expansion, as might be the case for a long constriction. After expansion in the divergent nozzle, recompression is accomplished by an inward-facing shock wave,[11] a more physically realistic process than the isentropic compression in Model 1.

Model 3 assumes that the incident flow stagnates behind a fully-reflected shock wave, a situation that is closely approximated for large values of A/A^*. However, since $u_6 = 0$, the continuity equation cannot be satisfied for the nozzle flow in this model. Here again, an inward-facing shock wave recompresses the steadily-expanded gas.

Based on our experience, we put forth Model 4 (see the Appendix) which uses an inward-facing shock wave in place of the isentropic compression used in Model 1, but is otherwise identical to Model 1. This inward-facing shock may locate itself in the divergent portion of the nozzle[5], or move downstream behind the transmitted shock[6].

---

12. *J. H. Spurk, E. J. Gion, and W. B. Sturek, "Investigations of Flow Properties in an Expansion Tube," BRL R 1404, Ballistic Research Laboratories, Aberdeen Proving Ground, MD, June 1968, (AD 673109). Also AIAA Paper No. 68-371, AIAA 3rd Aerodynamic Testing Conference, San Francisco, CA, April 1968.*

13. *O. La Porte, "On the Interaction of a Shock with a Constriction," Report LA 1740, Los Alamos Scientific Laboratory, Los Alamos, NM, 1954.*

IV. RESULTS FOR SINGLE VENTED PLATE

Results of the computations for a single vented plate are shown in Figures 3, 4, and 5.

In Figures 3 and 4, transmitted overpressure (T.O.) is plotted against incident overpressure (I.O.) for several area ratios. Figure 3 shows a graphical comparison between the computation models; Figure 4 gives more comprehensive computations for Model 4.

Each curve for models other than Model 4 is arbitrarily terminated at a point which we choose to call the "transition" point. As used here, this point, which will be different for each model, represents the set of conditions for which Model 4 predicts that the inward-facing shock will stand at the exit of the hypothetical nozzle; that is, where $M_c = M_7$ (See Appendix, Figure A1). To the left of this point, the shock stands somewhere in the divergent nozzle; to the right, it moves down the tube, following the transmitted shock wave. This right-hand segment is very nearly linear and can be closely approximated by a straight line out to values of incident overpressure (or incident Mach number) for which real gas effects become significant and a revised model is sometimes needed[6,12]. This linearity is evident for each of the other models as well.

Notice that the curves for Model 4 (Figures 3 and 4) do not pass through the origin as they should. The reason for this is that we stipulated sonic flow at the nozzle throat, thereby creating an artificial flow into the nozzle even for an acoustic wave (incident Mach number of unity, incident overpressure of zero). This assumption of the models is seen to have a small effect on the calculations; it is especially small at the larger area ratios. [However, it causes T.O./I.O. to become infinite as I.O. goes to zero, Figures 7a and 7b].

An estimate of the transmitted overpressure for an A/A* not shown on Figure 4 and a given incident overpressure, can be obtained by interpolating between the curves. But, interpolation is not strictly linear (see, for example, the curves for A/A* = 15, 20, and 25). A more useful representation[7] of the computed data (Model 4) for engineering purposes is shown in Figure 5. The abscissa is the fraction of blockage by the plate: it is zero when there is no restriction (T.O. = I.O.); and, it is unity when the restriction is a solid wall (T.O. = 0). Since the spacing between curves becomes smaller as I.O. increases, fewer curves are required than for Figure 4; and, at the higher values of I.O., linear interpolation between curves leads to small errors. This relatively weak dependence of T.O./I.O. on incident overpressure at moderate-to-large values will be shown more clearly later.

Some discrimination of such an estimate is sacrificed at high A/A* $(1-(A^*/A)\to 1)$, but we are primarily interested in A/A*<20 $(1-(A^*/A)< 0.95)$. Larger values of the area ratio are of little

practical interest, for, as seen in the insert on Figure 5, much of the shock attenuation possible is achieved before reaching high values of A/A*. For example, at A/A* = 20, 70-80% of the possible attenuation has been achieved for the range of incident overpressure considered.

The insert on Figure 5 also suggests that shock strength should be taken into account when selecting an area ratio for a desired attenuation level. For example, to achieve 70% attenuation of a 300 psi (2.07 MPa) wave, we need A/A* $\sim$ 20; whereas, for the same attenuation of a 60 psi (0.414 MPa) wave, we need only A/A* $\sim$ 12.5. However, this trend does not appear to be borne out by experiment[2,7].

A. Comparison of Models

1. Incident Flow

There are two conceptually different models for the incident flow -- Models 1 and 2 (Model 3 is actually a limiting case of Model 2). However, when we compared computed values for state [6'] of Model 1 with those of state [5] of Model 2, we found that they were the same within the accuracy of the plotted data (actually < 1% difference). Consequently, the two incident flow models are numerically equivalent, as alluded to by the results of Spurk *et al*[12] for the expansion tube.

We prefer the incident flow model of Model 1. Using it, we can compute flow conditions through to state [*] directly; whereas, an iterative solution is necessary to compute the strength of the partially reflected shock of Model 2. No substantial savings in machine time was realized by using the incident flow model of Model 1 for these calculations, because each complete calculation took only $\sim$ 0.07 seconds. However, substantial savings could be realized if similar calculations were done taking chemistry and real gas effects into account.

The effect of the two numerically-different incident flow models can be seen on Figure 3 by comparing Models 3 and 4, since Models 3 and 4 are identical except for their incident flow models. For each value of A/A*, the assumption of full reflection leads to a higher transmitted overpressure. In fact, at A/A* = 2, Model 3 predicts a transmitted overpressure which is larger than the incident overpressure. This results, because the full reflection model does not satisfy the continuity equation for flow into the nozzle. As a consequence of this violation, results are expected to be poor for small A/A* where velocity of flow into the nozzles can be significant. Improvement is expected as A/A* becomes larger and entry flow velocity becomes negligible. For example, the difference between Models 3 and 4 at 100 psi (0.689 MPa) is $\sim$ 15% for A/A* = 4, but decreases to $\sim$ 8.7% for A/A* = 8, and $\sim$ 4.3% for A/A* = 15. At even higher values of A/A* and higher incident overpressures, the differences between models can become negligibly small.

2. Long Constriction and Several Vent Holes

At $A/A^* = 4$ the comparison of models on Figure 3 includes Model 2 which accounts for the effect of a long constriction. Comparing Models 2 and 4, between which the only difference is the 'long constriction effect', we see that the effect is small--a percent difference of about 4% at "transition" and about 2% at 140 psi (0.965 MPa) incident overpressure. These differences are too small to measure with confidence. Experiment[7] shows that even in the actual case, where viscous effects would be included, the effect due to constriction length is small.

One analytic limitation of the simple models is that they cannot differentiate between a plate with a single vent hole having a certain area ratio and a plate with several vent holes having the same (effective) area ratio. However, experiments[2] have shown the differences in transmitted overpressure to be small.

3. Recompression Models

After the gas undergoes steady, isentropic expansion in the hypothetical nozzle, it is assumed to be recompressed by an isentropic process (Model 1), or by an inward-facing shock (e.g., Model 4). Since the incident flow model for Models 1 and 4 is the same, we can see the effect of the two recompression models by comparing their results on Figure 3. At the low area ratios, such as $A/A^* = 2$, where the entropy increase during recompression would be small, there is little difference between the models. But, as A/A^* increases and the amount of entropy increase during recompression becomes greater, the disparity between the results also becomes greater. For example, at $A/A^* = 2$, the difference is only $\sim 1.5\%$; at $A/A^* = 15$, it is $\sim 52.8\%$.

B. Comparisons with Experiment

1. Remarks on Experiments

The experiments we used for comparison with our computations, see Table I, were done in shock tubes for peaked waves[2,7] and step waves[4,5] incident upon single vented plates. (Pressure decays in time behind a peaked wave; it is uniform behind a step wave.) All plates, except for some used by Kingery[2], were vented by a single hole. Vent areas and incident overpressures of interest to different experimenters seldom overlapped, as shown in Table I.; and, data are scarce.

TABLE I - SOURCES OF EXPERIMENTS USED FOR SINGLE VENTED PLATE

SOURCE	MEASURED INCIDENT OVERPRESSURE (psig†)	TUBE DIA (cm)	TYPE INPUT WAVE	AREA RATIOS	LOCATION AND TYPE OF MEASURING STATION (Tube Dia's from Plate)
Kingery[2]	42, 113, 189	10.16	Peaked	2, 4, 10, 12.8	7 (Pressure)
Ross *et al*[7]	15, 30, 60, 75 90	91.44	Peaked	1.37, 2, 4, 8	13.2 & 19.4 (Shock Velocity)
Anet[4]	12.5, 15.5, 17.5, 28.4, 36.5	48.57	Step	8.2, 47.7, 94.5, 192.7, 487.5	2.2 (& 4.2) (Pressure)
Bertrand[5]	27, 85, 110	10.16	Step	23.3, 50.5, 96	12 to ∿ 60 (5 locations) (Pressure)

†*Multiply psi times 6.895 X 10^3 to get pressure in Pascals.*

In the experiments, pressure, or shock velocity (from which pressure can be computed), is measured ahead of and behind the vented plate. For experiments to be consistent with the computations, effects due to causes other than plate attenuation must be eliminated; that is, the tube must be calibrated so that the overpressure measured at a location behind the plate can be compared with the overpressure that would be measured there in the absence of the plate ($A/A^* = 1$). The latter is the equivalent incident overpressure. The data of Anet and Bertrand, which are not known to have been corrected thusly, will be used as published and as "corrected" assuming a 19% shock wave attenuation.

Because of the complex character of transmitted wave development, gage location may strongly influence the magnitude of the measured quantity. Measurements should be made far enough from the plate for transient effects to have become small. For example, for large area ratios and step waves of intermediate overpressure, Bertrand[5] found that the transmitted waves were peaked. Overshoot was quite large for their highest incident overpressures and area ratio, and persisted for $\sim$ 60 tube diameters, although it decayed to $\sim$ 10% of its average steady value within 30 tube diameters. At their lowest area ratio, $A/A^* = 23.3$, the overshoot was much smaller.

Another example of transient behavior was noted by Ross *et al*[7] for peaked incident waves which did not steepen to re-form as a transmitted plane shock front until they had traveled 5-10 tube diameters from the plate. Anet[4] also observed this non-steepening trend for weak step waves, but for $A/A^* \sim 200$.

For references 2, 5, and 7, even if transient effects have not abated, gage locations are such that each transient state should be comparable. This may not be true for the data of reference 4, since the gages are much closer to the plate. However, judging by the discussion above, differences may be small, especially at $A/A^* = 8.2$ where pressure overshoot should be small.

2. Comparisons

Figures 6 and 7 compare computations for Models 1 and 4 with measurements for several area ratios. The curves for Model 1 are again terminated at the "transition" point for Model 4.

On Figures 6a-f, Model 4 agrees best with measured transmitted overpressures over the entire range of area ratios and incident overpressures. It tends to predict higher values than were measured as incident overpressure increases, except at the higher area ratios. Overprediction is greatest at $A/A^* \sim 4$. The tendency to simplistically attribute the magnitude of this overprediction to dissipative effects should be resisted, because artificiality of the model also has an effect.

Figure 7 shows an important scaling effect noted in reference 7

and verified here for large-to-moderate incident overpressures by numerical computations: that the ratio of transmitted-to-incident overpressure is a weak function of incident overpressure. Actually, it appears that the measured ratio of overpressures is highest at the low incident overpressures and decreases to a nearly constant value as incident overpressure increases.

Here, again, we see that Model 4 predicts the measured values better than Model 1 over the full range of area ratios. The difference between the models becomes large for $A/A^* > 10$; at $A/A^* = 10$, it is 23% or more. The trend for measured values to fall below the prediction for incident overpressures greater than $\sim$ 60 psi (0.414 MPa) is reversed at the two highest area ratios.

Good agreement exists between the measurements of Kingery[2] and Ross *et al*[7] for peaked waves over a fairly wide range of incident overpressures. Also, no substantial difference is evident, for a rather narrow band of incident overpressures, between the data for peaked waves of Ross ($A/A^* = 8$) and that by Anet for step waves ($A/A^* = 8.2$). The validity of the latter comparison is, however, clouded by a noteable difference in measurement location and by an unsubstantiated correction used on Anet's incident overpressures.

V. RESULTS FOR A SERIES ARRAY OF PLATES

A. Experiment

An experiment was performed by Kingery[2] on a series array of 1/4 inch (6.35mm) thick vented plates placed 1/4 inch (6.35mm) apart. Five holes of 1/2 inch (12.7mm) diameter were drilled in the plates on a circle of 1 inch (25.4mm) radius with its center at the center of the 4 inch (10.16cm) diameter circular plate -- an area ratio for each plate of 12.8. In the experiment, peaked shock waves with nominal incident overpressure of 69 psi (0.476 MPa) [54 psi (0.372 MPa) equivalent incident overpressure] were incident upon first one plate, then upon arrays of two, three, and four plates in series. Incident pressure, pressure at the center of the last plate in the array, and transmitted pressure were measured for each array; results are in Table II. In addition, the build-up and decay of pressure between the plates was recorded by oscilloscope traces of the pressure gage output.

B. Computations and Comparison with Experiment

First, we applied the simple theory used for single plates to several plates in series by taking the wave transmitted by the first plate to be the wave incident upon the second plate. This procedure, which presupposes that spacing between the plates is large enough for a steady state to be reached, was repeated step-wise for each subsequent plate in the series. In this way, the overpressure

TABLE II - COMPARISON OF COMPUTATIONS (MODEL 4) AND EXPERIMENT FOR A 4- PLATE SERIES ARRAY OF VENTED PLATES†

		PLATE 1		PLATE 2		PLATE 3		PLATE 4	
	I.O. (psi)	$P_{6'}$ (psi)	T.O (psi)	$P_{6'}$ (psi)	T.O. (psi)	$P_{6'}$ (psi)	T.O. (psi)	$P_{6'}$ (psi)	T.O. (psi)
METHOD 1	54	234	14.7	55.1	4.0	23.6	1.3	17.4	1.2
METHOD 2	54	234	15.5	57.9	8.9	36.7	6.3	29.5	5.1
EXPERIMENT (Raw Data)	69	310	16.4	188	13.0	120	9.6	96	7.3
EXPERIMENT (Corr. Data)	54	234	16.4	141.9	13.0	90.6	9.6	72.5	7.3

†*Multiply psi times 6.895 X 10^3 to get pressure in Pascals.*

transmitted through each plate of the array was determined from a working graph of Model 4, such as Figure 4, for A/A* = 12.8. Maximum pressure on each plate was estimated by computing p_6 for the wave incident upon each plate (See Fig. 2a and Appendix A. Actually, we should use p_6', but for this area ratio, $M_6' \approx 0$, so $p_6' \approx p_6$). Results of this method are compared with experiment in Table II.

A second method, which should be more applicable to this experiment, is suggested by the hypothesis of Baker *et al*[14] that a series of vented plates, each with a vent area ratio α_i (i = 1, 2, ---, n) = $(A^*/A)_i$, behaves like a single plate with an effective area ratio given by

$$\frac{1}{\alpha_{eff}} = \frac{1}{\alpha_1} + \frac{1}{\alpha_2} + \text{---} + \frac{1}{\alpha_n} .$$

For this method, the appropriate effective area ratios for the single, two-, three-, and four-plate arrays are 12.8, 25.6, 38.4, and 51.2, respectively. Transmitted overpressure read for each array from Figure 5 are shown in Table II; p_6' was again computed as explained above, using the transmitted wave strength for subsequent plates.

Examination of Table II shows that agreement between experiment and computations is reasonably good for the single plate. For subsequent plates, agreement is poor for both methods--ample testimony that the computation model as used for the case of the single vented plate is inadequate for this series array of plates. [Computations would probably better agree with measurements for these closely-spaced plates if the assumption of choked flow were removed. It appears from the discussion in the next section that mass flow through the array is not a maximum, as the choked flow assumption stipulates. It seems reasonable that if the flow is not assumed to be choked, a lower transmitted overpressure would be computed.]

Method 1 results in much lower values than Method 2. But, Method 1 does not yield lower values than Method 2 for *all* A/A*. For example, it can easily be shown that for Model 4, two plates, each with A/A* = 2, transmit a higher pressure than a single plate with an effective A/A* = 4. Cross-over occurs at A/A* < ∿ 4, since two plates, each with A/A* = 4, transmit nearly the same pressure as a single plate with A/A* = 8. This observation is, of course, also true for Model 1 for which cross-over occurs at a slightly smaller value of A/A*.

---

14. *W. E. Baker, P. S. Westine, P. A. Cox, and E. D. Esparza, "Analysis and Preliminary Design of a Suppressive Structure for a Melt Loading Operation," SWRI Technical Report No. 1, Southwest Research Institute, San Antonio, TX, March 1974.*

Transmitted overpressure computed by Method 2 for the second through the fourth plates ranges from 30-35% lower than the measurements, but the pressure on each plate (p_6')is about a factor of three lower than the measurements (raw data). Even if we use the *measured* values of transmitted overpressure -- for which (from Figure 5) the arrays attenuate like single plates with area ratios of about 11.4, 15.6, 23.3, and 33.3, respectively -- the pressures computed from Equation (4) are still too low by factors of 2.5-3 (corrected data). [We feel justified in using the equations without "viscous" correction for the 4-plate case, because loss terms did not appear to be a factor in the comparison of computations with experiment for one plate below $\sim$ 60 psi (0.414 MPa) (see Figure 6).]

C. Other Observations

Examination of the magnitude and shape of oscilloscope traces[2] of incident and transmitted wave pressures, and of pressures between the three arrays of closely-spaced plates, shows that between the plates, expansion of the transmitted wave is incomplete (its magnitude lies between the computed values for p* and p_6'), and that it never regains its shock-like shape until it leaves the last plate.

In essence, fluid appears to "leak" through the arrays in a way shown on Figure 8, which is a representation from the oscilloscope traces of the pressure on each plate at a particular instant in time. The time t_o is the time at which the pressure on the first plate is a maximum; t_2, t_3, and t_4 are the approximate times (after t_o) at which the pressures on plates 2, 3, and 4, respectively, reach a maximum.

At t_1 we see that a pressure wave has been transmitted through the 4-plate array very quickly -- in about one-tenth the time required for the pressure on plate 4 to peak. During this transit time, the pressure on the first plate has decreased only $\sim$ 7% from its peak value. This observation suggests that computations such as ours, which are, strictly speaking, applicable only to step waves, should also be applicable to transmission of a peaked wave with the same maximum incident pressure. The agreement, for single plates, between the data measured for a peaked wave ($A/A^* = 8$) and a step wave ($A/A^* = 8.2$) on Figure 6c seems to bear out this point, although data are insufficient for firm conclusions to be made.

In principle, we should also be able to compute the decay history of the transmitted pressures between and behind the plates by approximating the incident wave as a series of step waves of decreasing amplitude, because the transmitted wave is directly coupled to the incident wave to experimental accuracy. This has been shown by

scaling down the magnitude of incident waves from reference 7 and incident reflected waves from reference 2 using the ratio of peak transmitted to peak incident wave pressures, and then comparing the *resulting* "transmitted" wave shapes with the *measured* transmitted wave shape. Of course, we recognize that such an approximation is an over-simplication of the actual time-dependent, three-dimensional flow situation, but it may be useful. The main drawbacks of this simplistic approach are that the models simply do not predict the *magnitude* of the pressures accurately enough, and that the time when maximum pressure is attained cannot be approximated accurately (for example, from the known distance and an average of the computed velocities.

VI. CONCLUDING REMARKS

Several steady, one-dimensional models of the interaction of a shock wave with vented plates have been compared with each other and with experiment. These models have one basic tenet in common -- simplicity. One model, Model 4, was formulated to combine the preferred features of the models: 1) Its entry model gave the same entry conditions as the partial reflection model, without requiring an iterative solution -- a potential time-saver. Allowing for partial reflection was shown to have a noticeable influence on transmitted overpressure at low-to-moderate A/A*; and 2) Computations were greatly simplified by replacing the actual transient, three dimensional expansion of the flow from the vent hole(s) by a hypothetical steady expansion in a quasi-one-dimensional divergent nozzle. The credibility of Model 4 was enhanced by the fact that its expansion model assumed a transmitted shock-structure consistent with the steady-state situation observed when a free jet expands from a tubular restriction into a larger tube[10]. That is, the transmitted shock wave was followed (for some conditions, see Appendix) by an inward-facing (recompression) shock wave.

Again, it should be stressed that the location of the measurement point downstream of the vented plate can be very important when measurements are being compared with computations. For example, for the 4-plate series array, the pressure was measured on the back of plate 4 to be 15.4 psi (0.106 MPa). If that pressure were used in conjunction with Figure 5, the array would appear to attenuate like a single plate with an effective area ratio, $A/A^* = 13.3$. This value is only slightly larger than the area ratio for each individual plate and quite different from the effective value of ~ 37 computed for the pressure measured farther downstream. In making our comparisons, we tried to use consistent data (see earlier discussion of Table I).

Specific conclusions based on this work are:

For a single vented plate:

1) The number of computations is greatly reduced by the

fact that, for a given A/A*, transmitted overpressure versus incident overpressure can be represented by a straight line (for a certain region -- see earlier discussion of Figure 4), and by the fact that the ratio of transmitted-to-incident overpressure is nearly constant over a wide range of interest (Figures 7a and 7b). The latter fact also reduces the number of experiments needed. 2) Model 4 agrees adequately with shock tube measurements of transmitted overpressure for fairly low incident overpressures (See Figures 6a-6f). For incident overpressures above "transition" from the hypothetical nozzle, a correction term is needed. 3) The models are applicable to step waves, but can be applied to peaked waves if the shape of the incident wave is known. 4) More -- and more careful -- data are needed to resolve the differences between computed and measured ratios of transmitted-to-incident overpressures at low incident overpressures (See Figures 7a and 7b), although our current interest in this region is small.

For a series array of vented plates:

1) These simple models cannot be applied with profit to the transmission of a shock wave by closely-spaced plates, since transient effects are obviously important. Neither of the two methods we tried (See Table II) predicted the peak pressure between plates adequately. The method using equivalent area ratio predicted the transmitted pressure best, but its predictions were still below the measured values, in contrast to expectations. 2) The experiment presently available is not a valid test for the models. Plates should have wider separation so that steady-state conditions will be approached. However, for most practical vented structures, the elements of the structure will likely be closely-spaced. [Unfortunately, data available in reference 3 for more widely-spaced plates did not include pressure measurements between the plates.] 3) For closely-spaced plates, experiment or a three-dimensional transient ("filling") code is required. Some simplification of the codes may be possible by taking advantage of the coupling between incident and transmitted wave decay mentioned earlier. Computations by Proctor[15] using their hydro-code show the expected trends for filling between plates of a 4-plate array for peaked and step incident waves.

VII. RECOMMENDATIONS

It is recommended that:

1) Figure 5 be used to estimate the transmitted overpressure for given incident overpressure and A/A*. 2) An experiment be done for widely-spaced plates (same plates, same incident wave strength)

---

15. *Private communication from Mr. J. F. Proctor, Naval Surface Weapons Center, White Oak Laboratory, Dahlgren, VA, October 1975.*

to see if our model is appropriate for that case. And, an experiment be done for the 4-plate array at a higher incident overpressure, where losses appear to be greater. 3) The feasibility of relaxing the choked flow assumption be examined; and, if it is feasible, calculations be done for a series array of plates and compared with experiment. 4) An experiment be done with step waves incident upon single and multiple-plate arrays to quantify the effect of a step wave as opposed to a peaked wave on pressure between the plates. 5) The feasibility of simplifying applicable hydro-codes by assuming direct coupling between the decay of the transmitted wave and the known decay of the incident wave be examined; a considerable saving of computation time may be realizable.

ACKNOWLEDGMENTS

The help of Dr. Kevin S. Fansler, who programmed Model 4 for the computer, is gratefully acknowledged. Discussions with Dr. C. W. Kitchens regarding flow through the series array of plates are also gratefully acknowledged.

ADDENDUM

Analysis of some of the data referred to in reference 2 was completed after completion of this report. An empirical relationship was found assuming that the ratio of transmitted-to-incident overpressure is a function of area ratio alone. That relationship[16], $T.O./I.O. = 1.164\ (A/A^*)^{-0.5135}$, is shown plotted on Figure 5 (insert). It is a least squares fit to data for single plates with vent area ratios from 2 to $\sim$ 20.

It is also noteworthy that Kingery[2] found good agreement between transmitted overpressures (T.O.) measured behind two-, three-, and four-plate arrays and transmitted overpressures computed for corresponding incident overpressures (I.O.) using the above equation. The area ratio for each array was computed using the equation on page 18 of this report.

---

16. *C. Kingery and G. Coulter, "Shockwave Attenuation by Single Perforated Plates," BRL Memorandum Report (to be published), Ballistic Research Laboratories, Aberdeen Proving Ground, MD.*

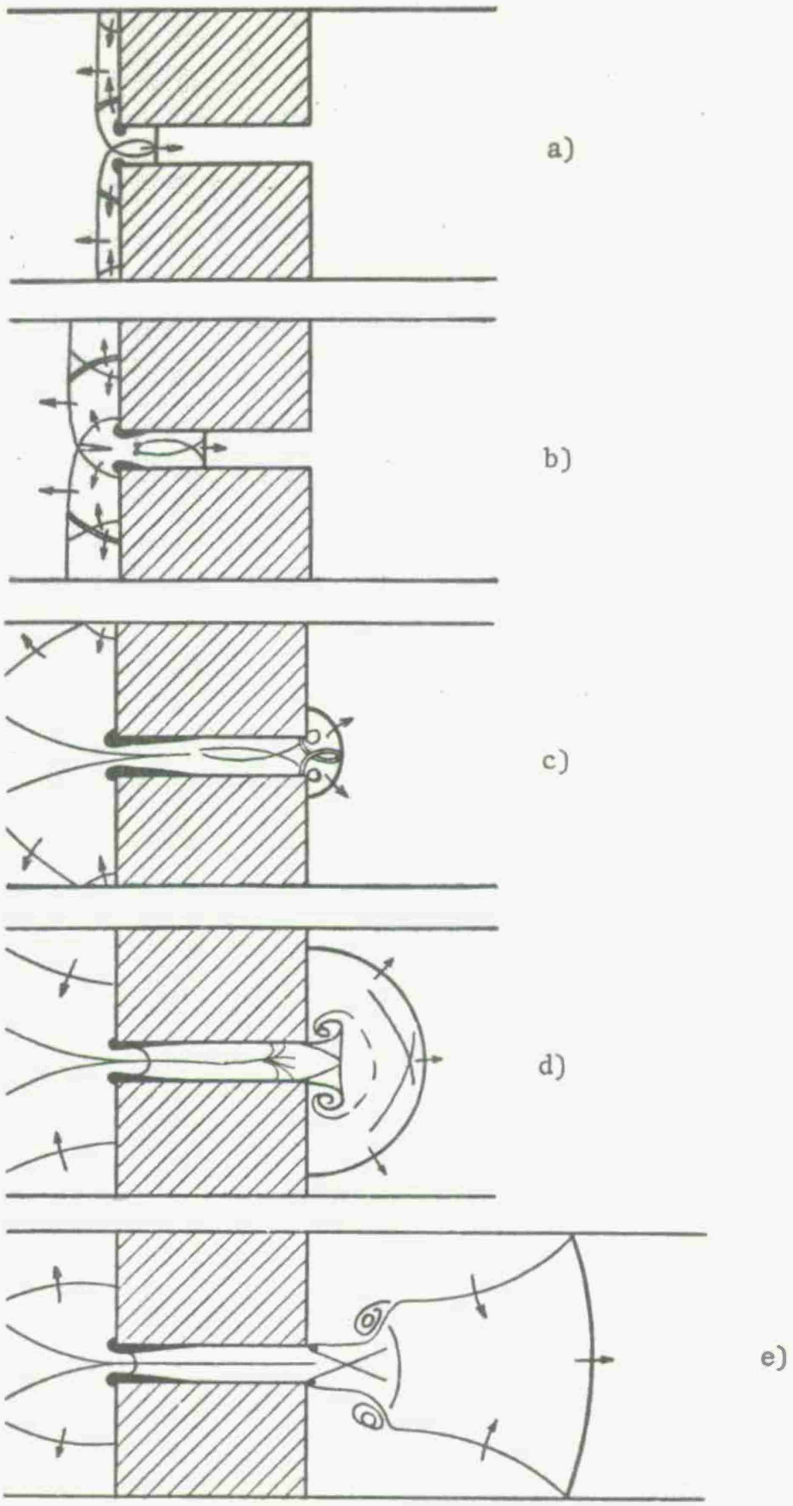

Figure 1. Stages During the Transmission of a Shock Wave Through a Single Slit in a Plate after Reference 4.

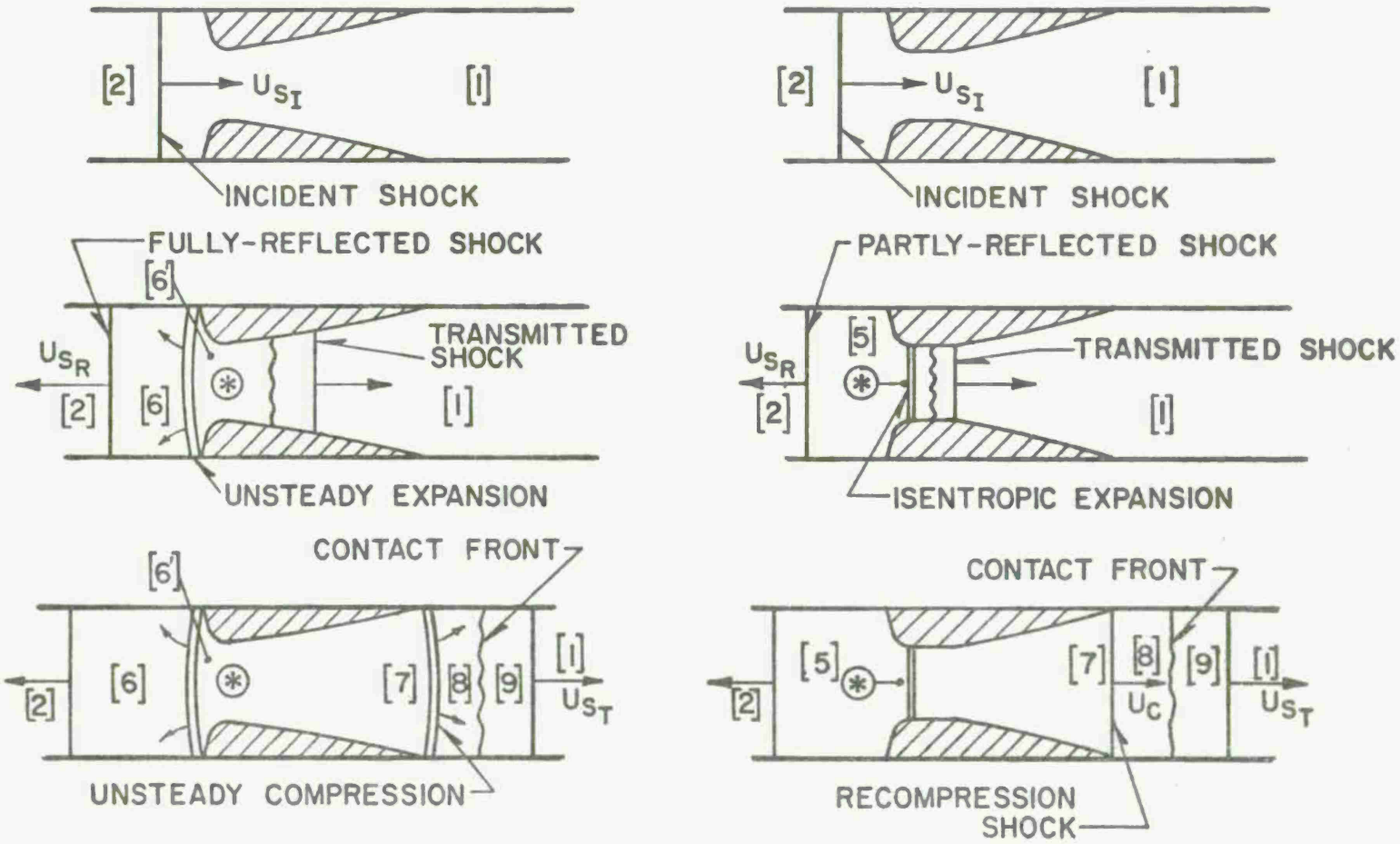

a) Model 1 b) Model 2

Figure 2. Sketches of Flow Models. Flow processes are symbolic only.

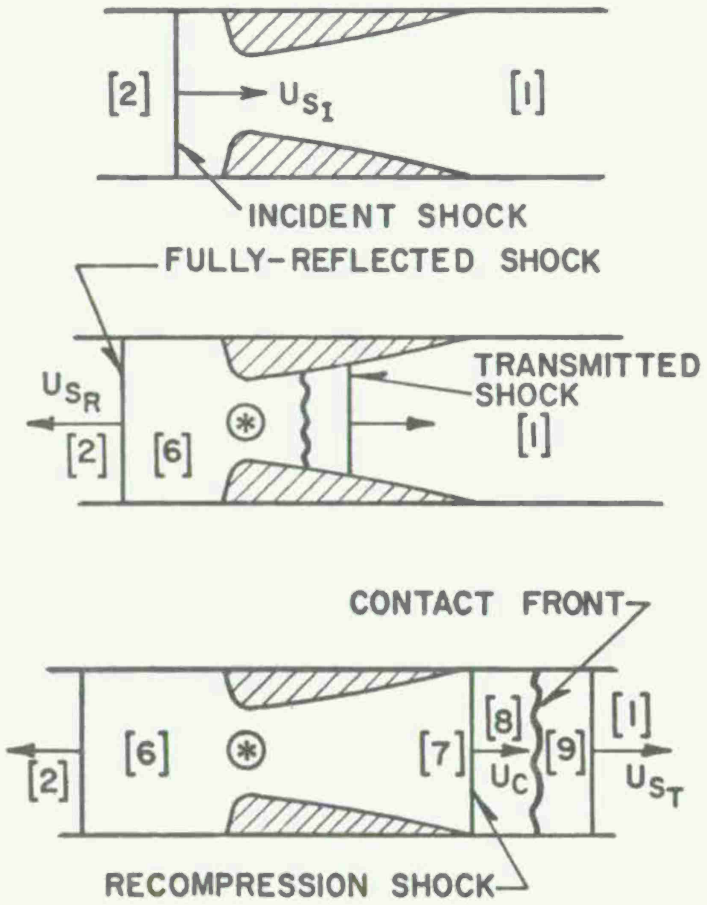

c) Model 3

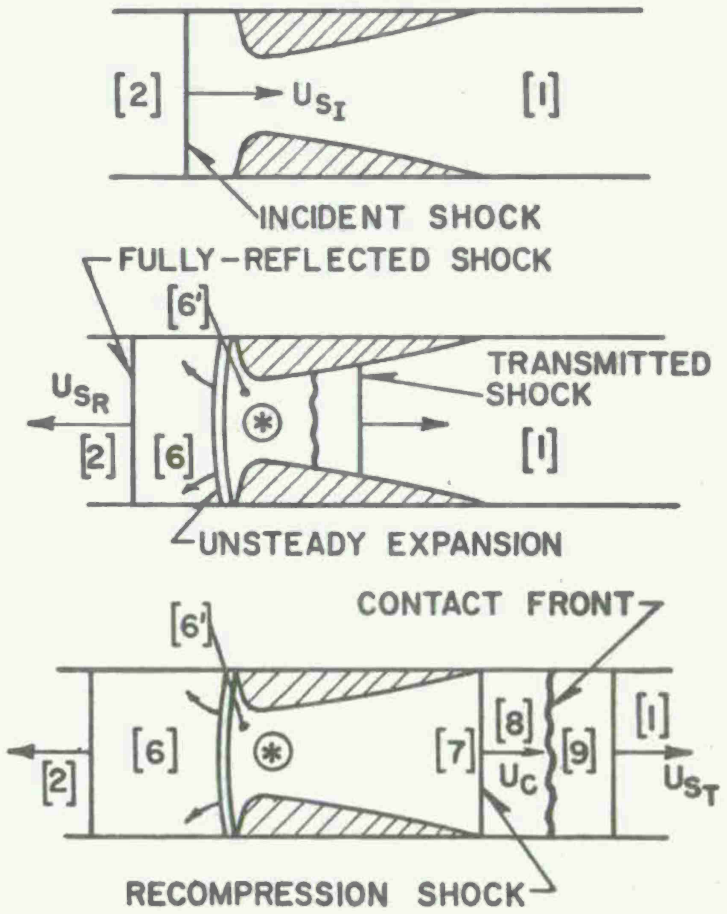

d) Model 4

Figure 2. Sketches of Flow Models. Flow processes are symbolic only.

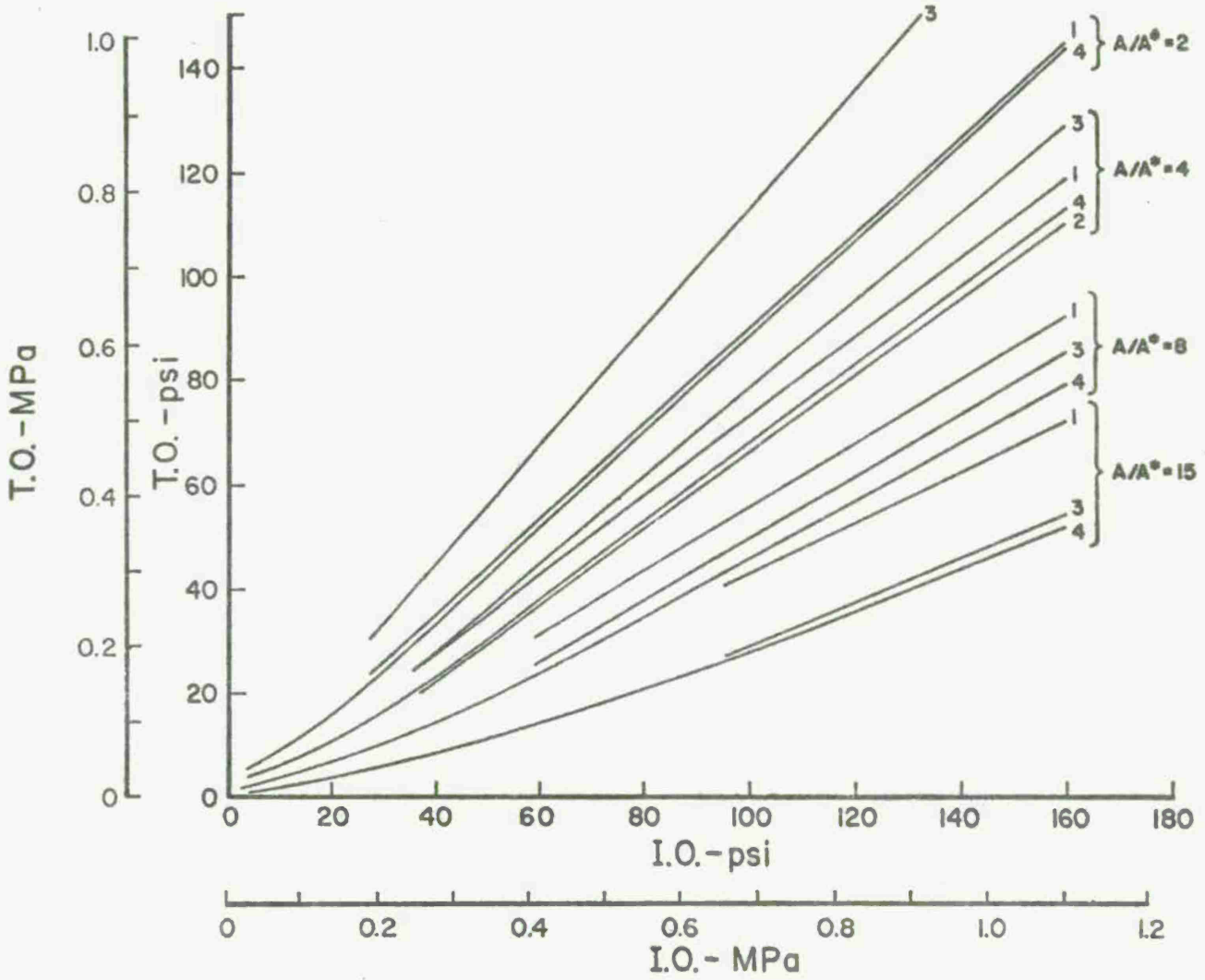

Figure 3. Comparison of Transmitted Overpressure (T.O.) Versus Incident Overpressure (I.O.) for Flow Models, A/A* = 2,4,8, and 15. 1,2,3, and 4 refer to models 1,2,3, and 4 respectively. Pressure is given in pounds per square inch (psi) and in millions of Pascals (MPa).

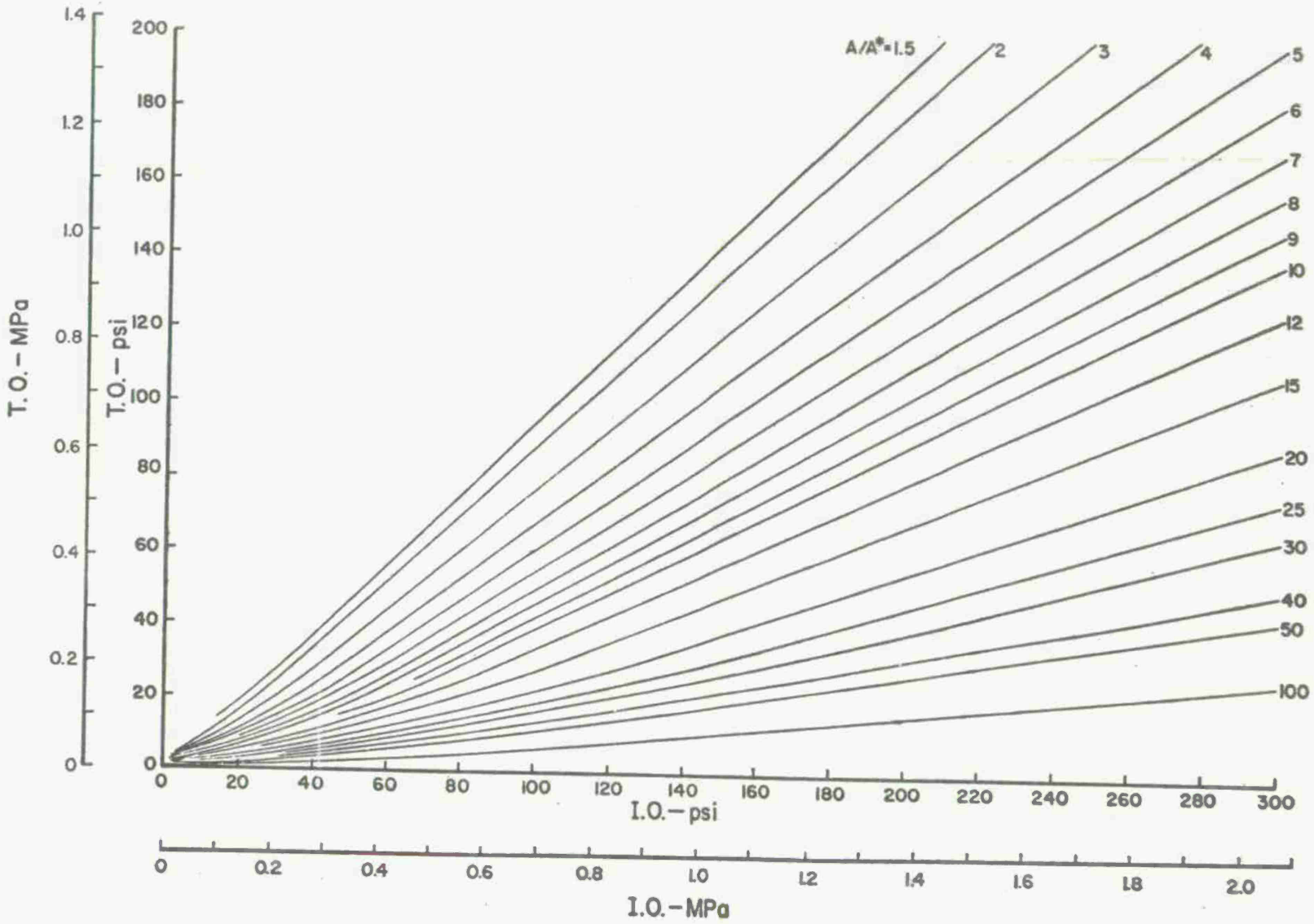

Figure 4. Transmitted Overpressure (T.O.) Versus Incident Overpressure (I.O.) for Model 4; A/A* = 1.5 -100.

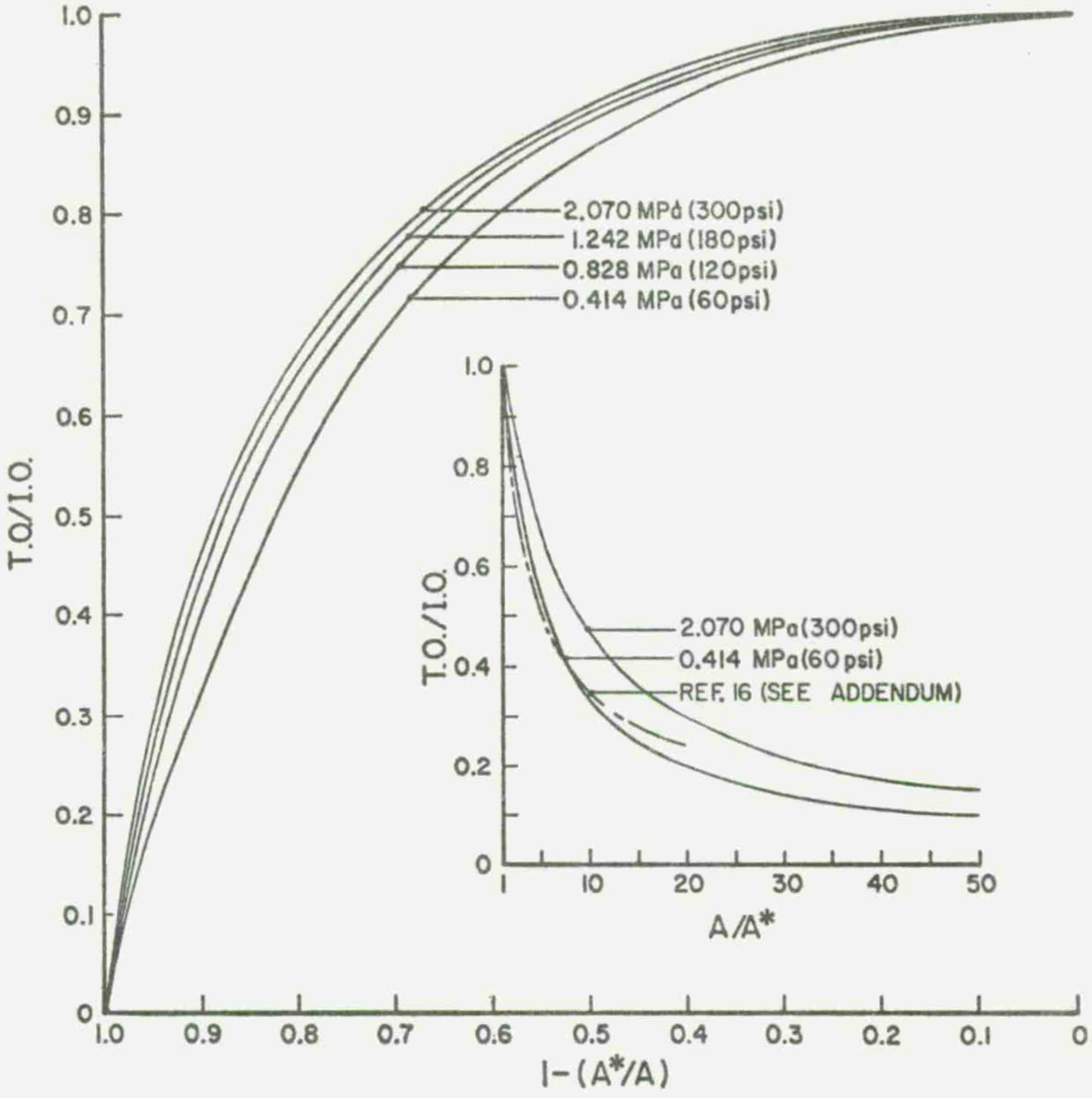

Figure 5. Ratio of Transmitted-to-Incident Overpressure (T.O./I.O.) Versus Fraction of Blockage by the Plate for Model 4. Insert: T.O./I.O. Versus Area Ratio. The free parameter is incident overpressure in millions of Pascals.

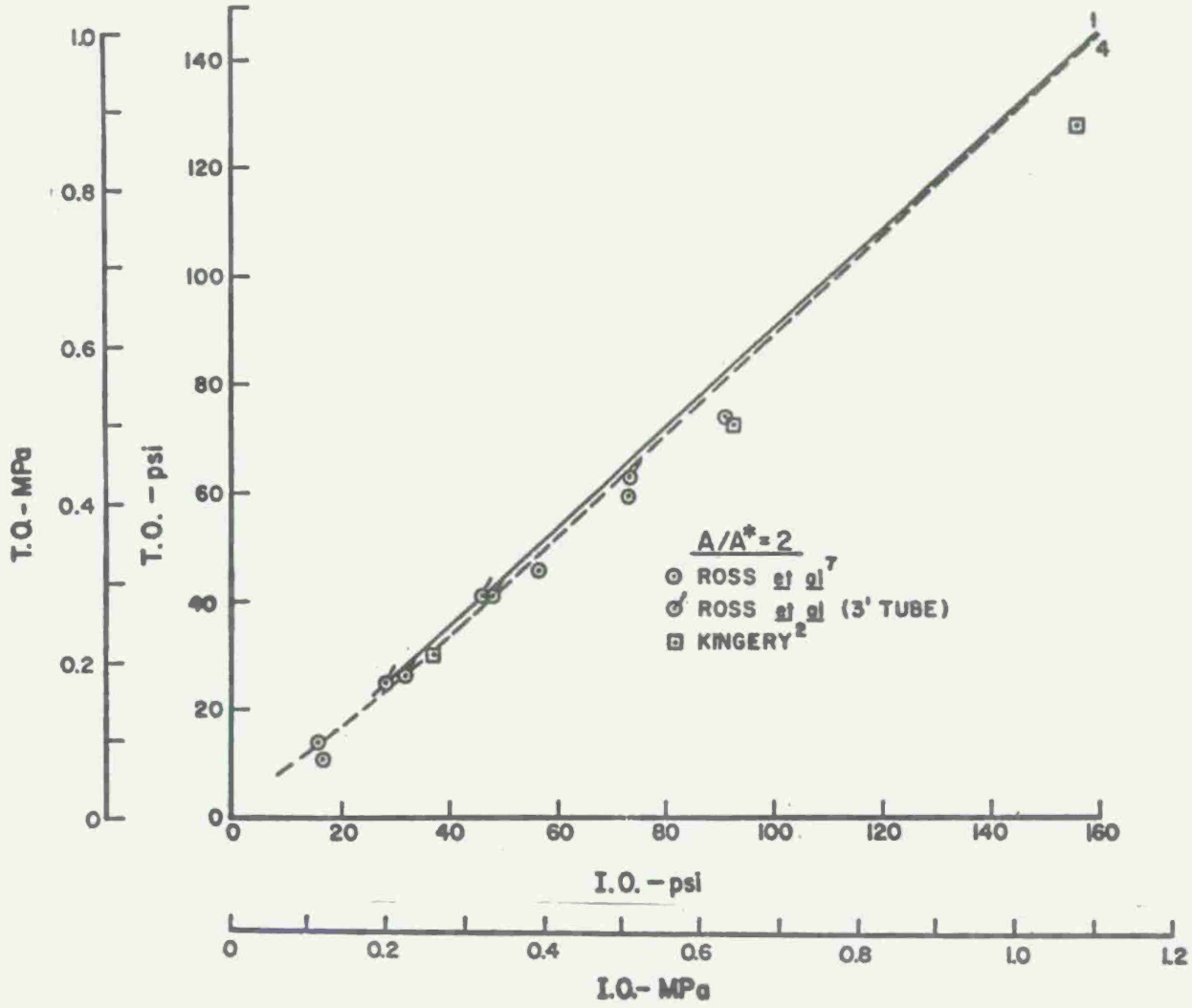

Figure 6a. Comparison of Experiment with Models 1 and 4: Transmitted Overpressure (T.O.) Versus Incident Overpressure (I.O.) for A/A* = 2.

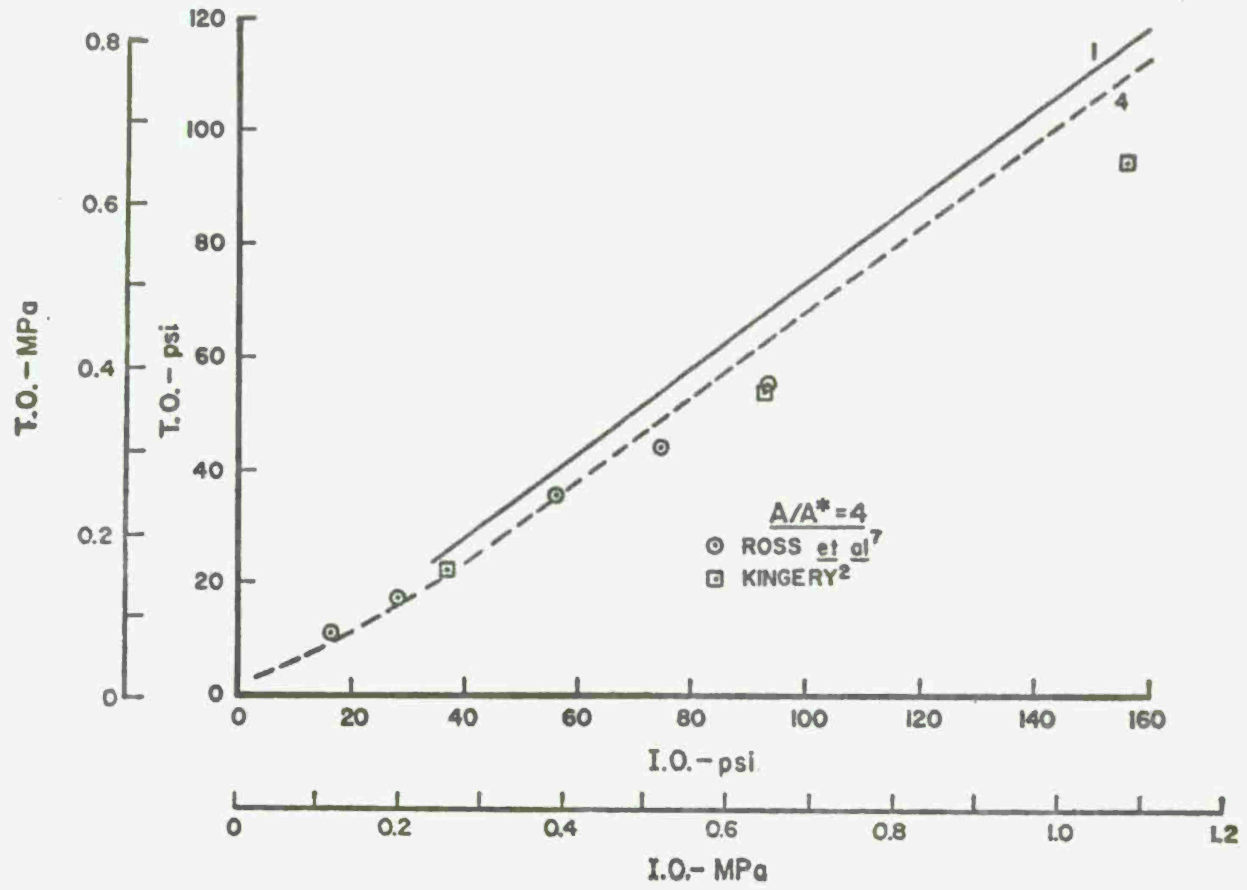

Figure 6b. Comparison of Experiment with Models 1 and 4: Transmitted Overpressure (T.O.) Versus Incident Overpressure (I.O.) for A/A* = 4.

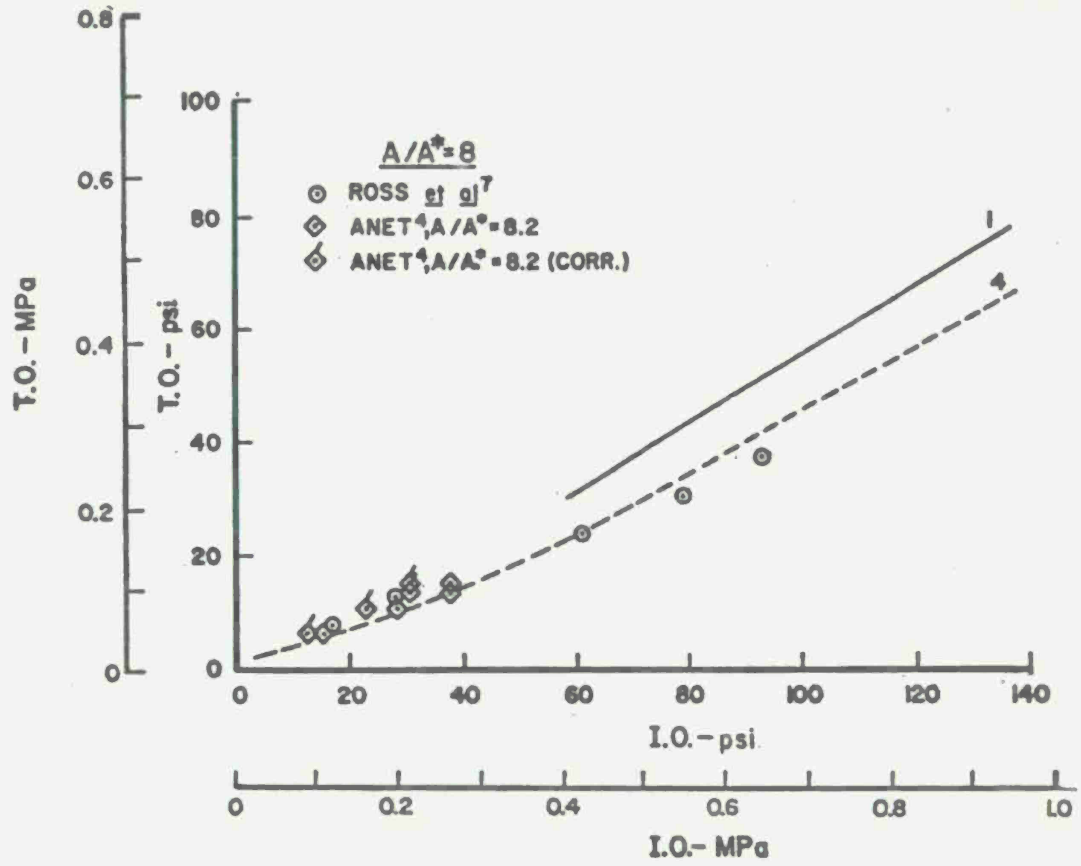

Figure 6c. Comparison of Experiment with Models 1 and 4: Transmitted Overpressure (T.O.) Versus Incident Overpressure (I.O.) for A/A* = 8.

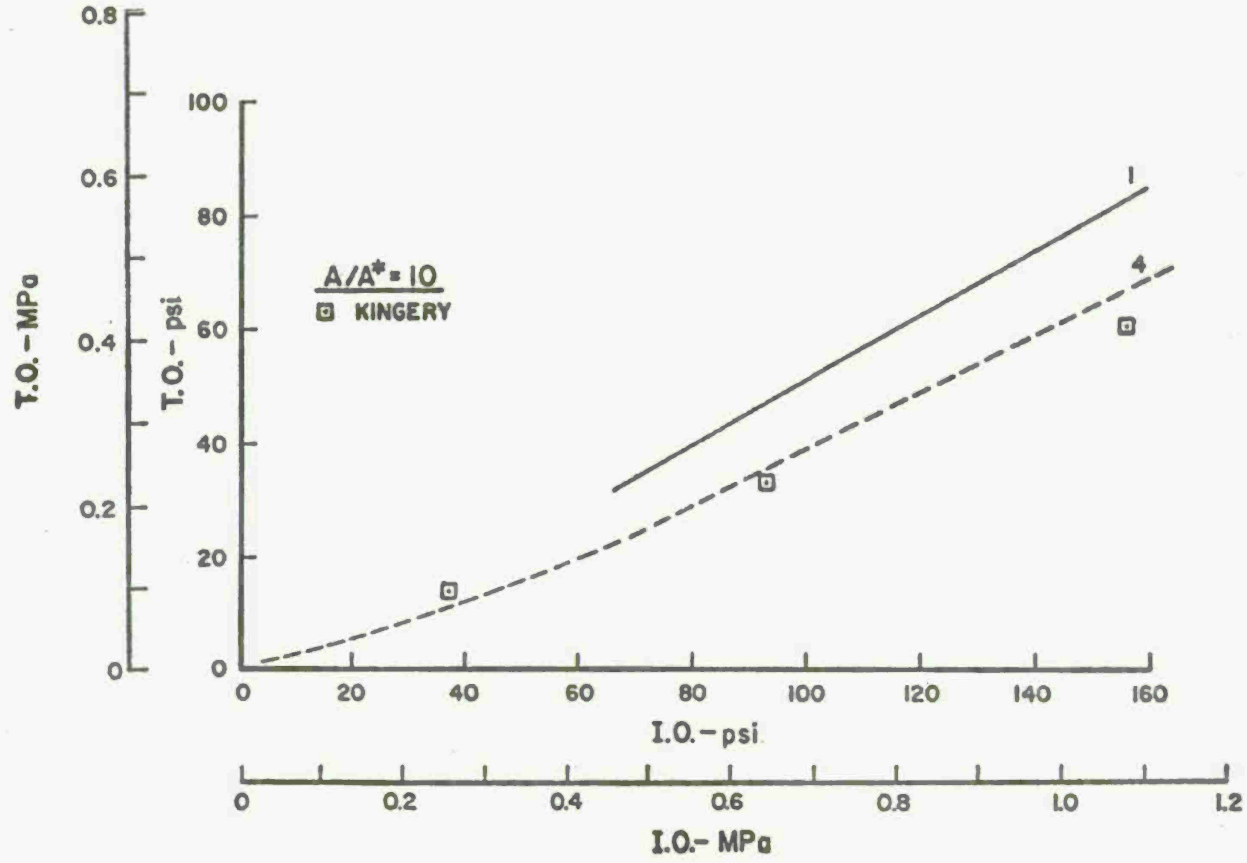

Figure 6d. Comparison of Experiment with Models 1 and 4: Transmitted Overpressure (T.O.) Versus Incident Overpressure (I.O.) for A/A* = 10.

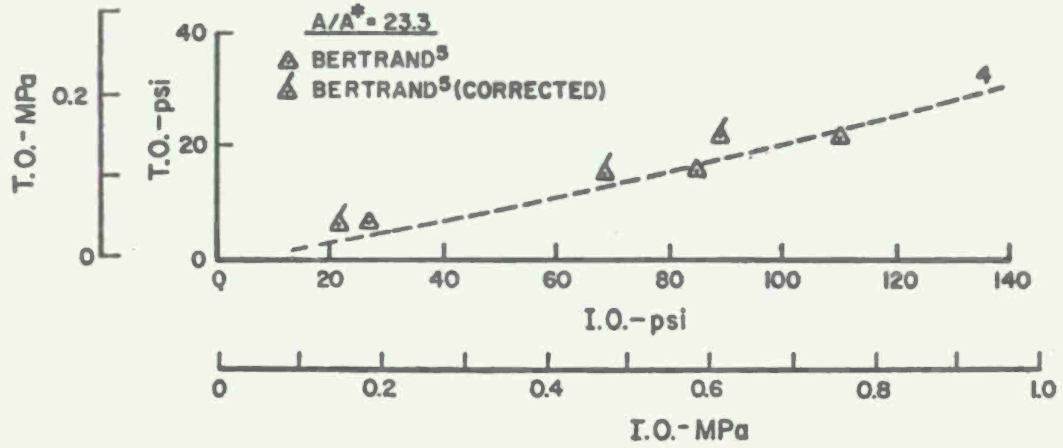

Figure 6e. Comparison of Experiment with Model 4: Transmitted Overpressure (T.O.) Versus Incident Overpressure (I.O.) for A/A* = 23.3.

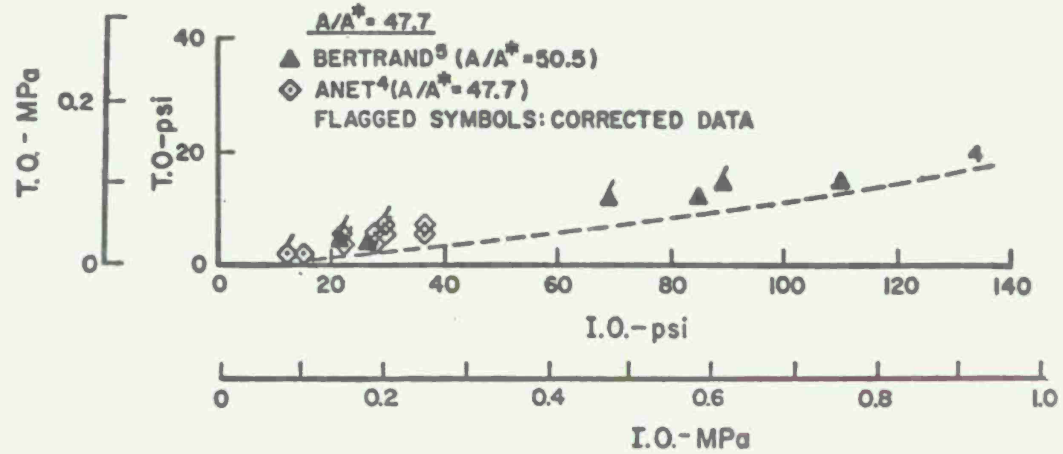

Figure 6f. Comparison of Experiment (A/A* = 47.7, 50.5) with Model 4 (A/A* = 47.7): Transmitted Overpressure (T.O.) Versus Incident Overpressure (I.O.).

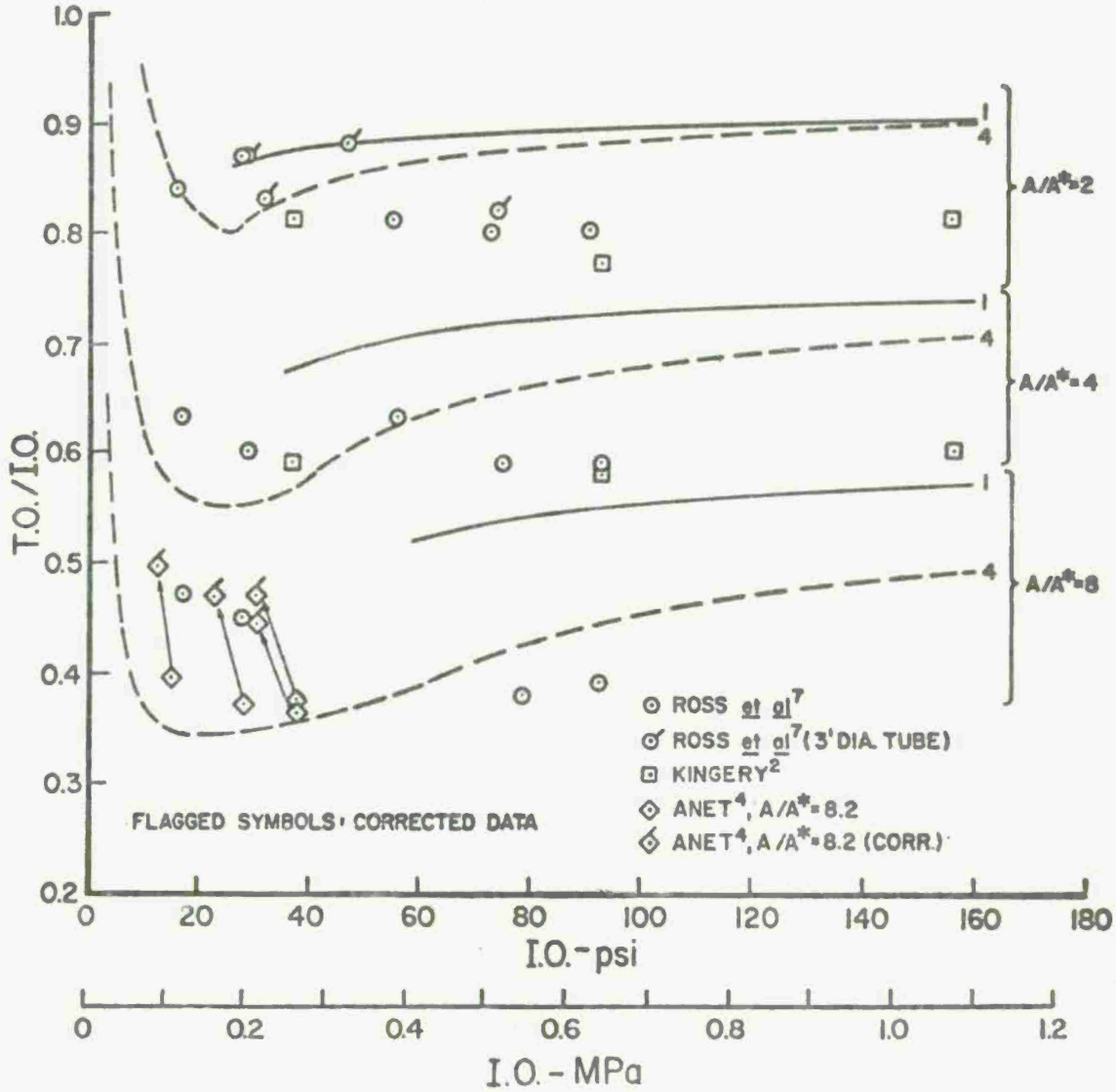

Figure 7a. Comparison of Experiment with Models 1 and 4: Ratio of Transmitted-to-Incident Overpressure (T.O./I.O) Versus Incident Overpressure; A/A* = 2, 4, and 8. Arrows indicate the shift when data assumed to be uncorrected are corrected as per discussion on page 15.

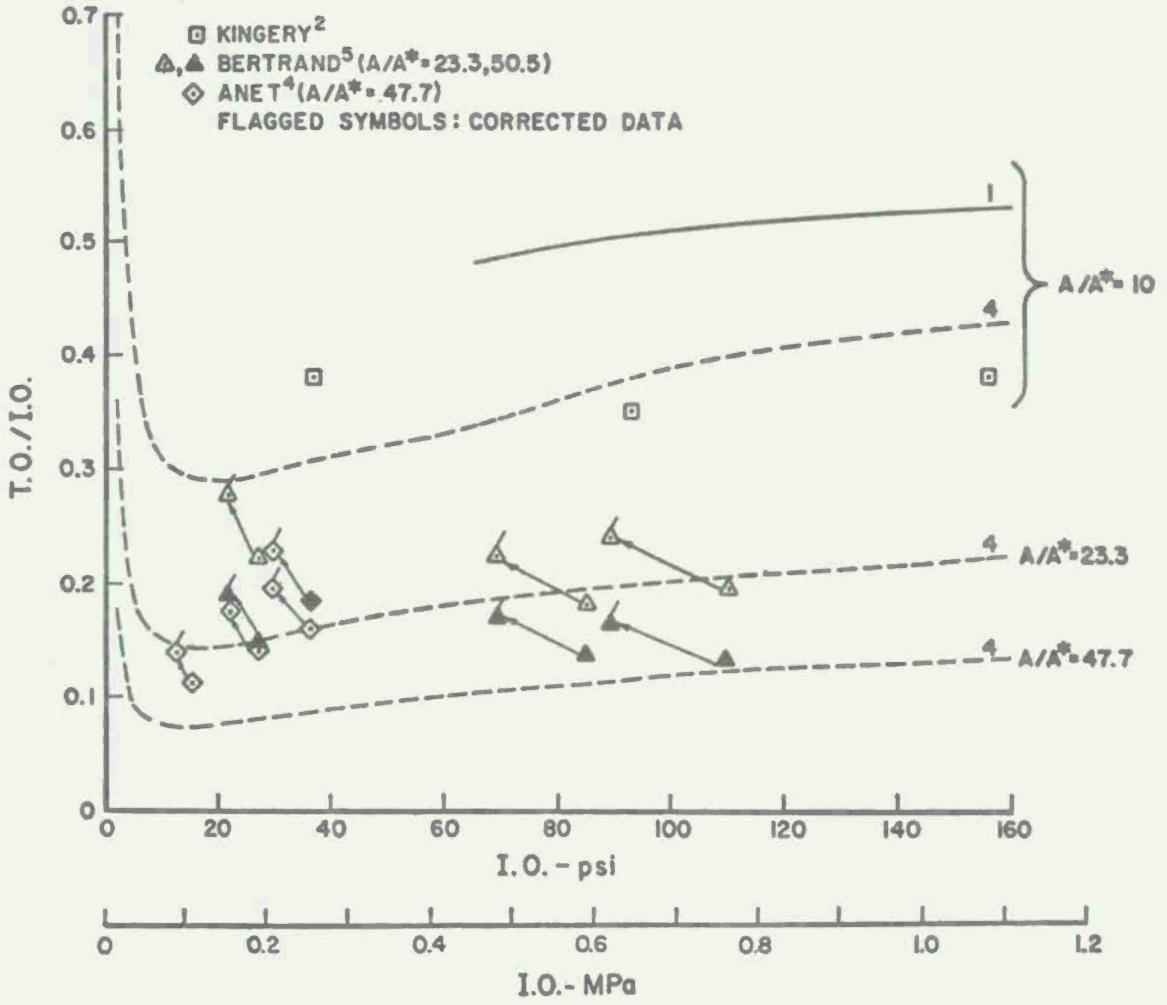

Figure 7b. Comparison of Experiment with Models 1 and 4: Transmitted Overpressure (T.O.) Versus Incident Overpressure (I.O.) for A/A* = 10, 23.3, and 47.7 (and 50.5). Arrows indicate the shift when data assumed to be uncorrected are corrected as per discussion on page 15.

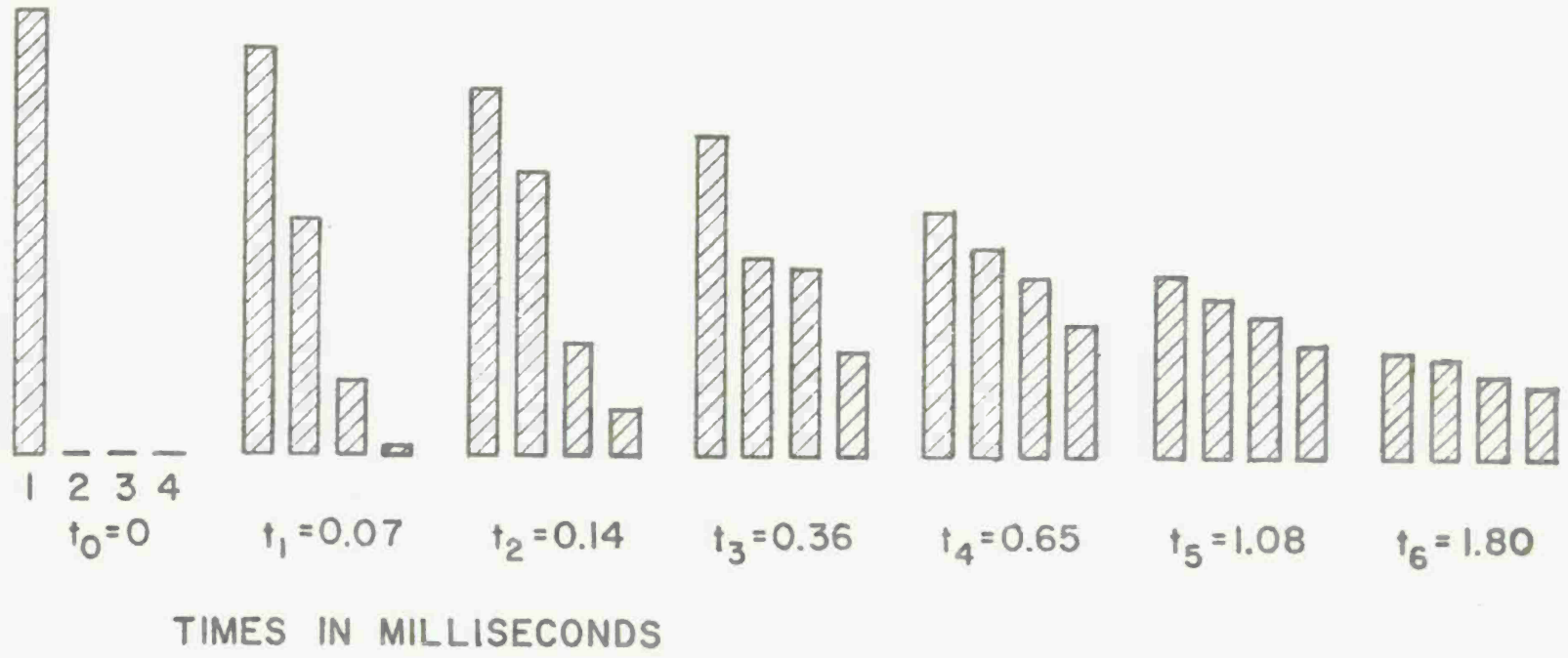

Figure 8. Pressure Measured at Several Instants in Time Between the Plates of a 4-Plate Series Array. The numbers 1, 2, 3, and 4 at t_o are the plate numbers. The incident overpressure, pressure at t_o, is 234 psi(1.61 MPa).

REFERENCES

1. C. Kingery, R. Schumacher, And W. Ewing, "Internal Pressures from Explosions in Suppressive Structures," BRL IMR 403, Ballistic Research Laboratories, Aberdeen Proving Ground, MD., June 1975.

2. Private communication from Mr. C. Kingery, Ballistic Research Laboratories, Aberdeen Proving Ground, MD., November 1975.

3. L. Dresner and C. V. Chester, "Attenuation of Shocks in Tubes by Orifice Plates," ORNL - TM-1750, Oak Ridge National Laboratory, Oak Ridge, TN., 1967.

4. B. Anet, "Experimentelle Untersuchung über den Einfluss einer Einschnürung auf die Stosswellenausbreitung in einem Kanal Konstanter Querschnitts," Bericht SHB Nr. 68-17-G3, Studienkommission des EJPD für Zivilschutz, Zürich, Switzerland, 1968.

5. B. P. Bertrand, "Shock Wave Transmission through a Large Restriction in a Constant Area Duct," BRL MR 1848, Ballistic Research Laboratories, Aberdeen Proving Ground, MD., June 1967 (AD 656744).

6. L. L. Monroe, "Investigation of the Transmission of a Shock Wave through an Orifice," GALCIT Hypersonic Research Project Memorandum No. 46, Guggenheim Aeronautical Laboratory, California Institute of Technology, Pasadena, CA.,September 1958.

7. J. M. Ross, C. M. Nixon, and W. M. McMurtry, "A Shock Tube Study of Attenuation of Air Flow through Chokes," Suffield Technical Note No. 152, Suffield Experimental Station, Ralston Alberta, Canada, May 1966.

8. F. H. Oertel, N. Gerber, and J. M. Bartos, "The Modified Expansion Tube: Theory and Experiment," BRL R 1741, Ballistic Research Laboratories, Aberdeen Proving Ground, MD., September 1974 (AD A001551).

9. E. M. Schmidt and D. D. Shear, "The Flow Field About an M-16 Rifle," BRL R 1692, Ballistic Research Laboratories, Aberdeen Proving Ground, MD., January 1974 (AD 916646L). Also "The Formation and Decay of Impulsive, Supersonic Jets," AIAA Paper No. 74-531, AIAA 7th Fluid and Plasma Dynamics Conference, Palo Alto, CA.,June 1974.

10. F. H. Oertel, Jr., "Laser Interferometry of Unsteady, Underexpanded Jets," BRL R 1694, Ballistic Research Laboratories, Aberdeen Proving Ground, MD., January 1974 (AD 773664).Also Proc. Int'l. Cong. Instr. in Aerospace Simulation Facilities, CA Institute of Technology, Pasadena, CA.,September 1973.

11. G. Rudinger, Nonsteady Duct Flow: Wave-Diagram Analysis, Dover Publications, Inc., New York, N.Y., 1969, p. 94.

12. J. H. Spurk, E. J. Gion, and W. B. Sturek, "Investigations of Flow Properties in an Expansion Tube," BRL 1404, Ballistic Research Laboratories, Aberdeen Proving Ground, MD, June 1968, (AD 673109). Also AIAA Paper No. 68-371, AIAA 3rd Aerodynamic Testing Conference, San Francisco, CA.,April 1968.

13. O. La Porte, "On the Interaction of a Shock with a Constriction," Report LA 1740, Los Alamos Scientific Laboratory, Los Alamos, NM.,1954.

14. W. E. Baker, P. S. Westine, P. A. Cox, and E. D. Esparza, "Analysis and Preliminary Design of a Suppressive Structure for a Melt Loading Operation," SWRI Technical Report No. 1, Southwest Research Institute, San Antonio, TX.,March 1974.

15. Private communication from Mr. J. F. Proctor, Naval Surface Weapons Center, White Oak Laboratory, Dahlgren, VA.,October 1975.

16. C. Kingery and G. Coulter, "Shockwave Attenuation by Single Perforated Plates," BRL Memorandum Report (to be published), Ballistic Research Laboratories, Aberdeen Proving Ground, MD.

APPENDIX: GOVERNING EQUATIONS FOR MODEL 4

Approach

The shock wave approaching the vented structure is governed by the jump relations. For a given Mach number, $M_{S_I} \equiv U_{S_I}/a_1$ (see Fig. 2), the equations in a shock-fixed coordinate system are:

$$\frac{u_2}{a_1} = \frac{2}{\gamma+1}\left(M_{S_I} - \frac{1}{M_{S_I}}\right) \tag{1}$$

$$Y_I \equiv \frac{p_2}{p_1} = \frac{2\gamma}{\gamma+1} M_{S_I}^2 - \frac{\gamma-1}{\gamma+1} \tag{2}$$

$$\frac{a_2}{a_1} = \left\{ \frac{Y_I \left(Y_I + \frac{\gamma+1}{\gamma-1}\right)}{\frac{\gamma+1}{\gamma-1} Y_I + 1} \right\}^{1/2} \tag{3}$$

Entry

As in reference 8, we assume that the shock wave is fully-reflected from the plate, and that flow into the hypothetical nozzle is established by an unsteady expansion to the state[6′] (see Fig. 2a). Again in a shock-fixed coordinate system, the governing equations across the reflected shock are:

$$Y_R \equiv \frac{p_6}{p_2} = \frac{\left(\frac{\gamma+1}{\gamma-1} + 2\right) Y_I - 1}{Y_I + \frac{\gamma+1}{\gamma-1}} \; ; \qquad \frac{p_6}{p_1} = Y_R \cdot Y_I \tag{4}$$

$$\frac{a_6}{a_2} = \left\{ \frac{Y_R \left(Y_R + \frac{\gamma+1}{\gamma-1}\right)}{\frac{\gamma+1}{\gamma-1} Y_R + 1} \right\}^{1/2} \; ; \qquad \frac{a_6}{a_1} = \frac{a_6}{a_2} \cdot \frac{a_2}{a_1} \tag{5}$$

For the unsteady, isentropic expansion, we have from the Riemann condition, $u + \frac{2}{\gamma-1} a = \text{const}$, and the isentropic relation, $p = \text{const} \cdot \rho^{\gamma} = \text{const} \cdot a^{2\gamma/\gamma-1}$:

$$\frac{a_{6'}}{a_1} = \frac{a_6/a_1}{1 + \frac{\gamma-1}{2} M_{6'}} \quad ; \qquad u_6 = 0 \tag{6}$$

$$\frac{u_{6'}}{a_1} = M_{6'} \cdot \frac{a_{6'}}{a_1} \tag{7}$$

$$\frac{p_{6'}}{p_1} = \frac{p_{6'}}{p_6} \cdot \frac{p_6}{p_1} = \left\{ \frac{a_{6'}/a_1}{a_6/a_1} \right\}^{\frac{2\gamma}{\gamma-1}} \cdot \frac{p_6}{p_1} \tag{8}$$

where we compute $M_{6'} < 1$ from the equation for steady nozzle flow:

$$\frac{\left(M_{6'}^2 + \frac{2}{\gamma-1}\right)^{\frac{\gamma+1}{2(\gamma-1)}}}{M_{6'}} = \frac{\left(M_7^2 + \frac{2}{\gamma-1}\right)^{\frac{\gamma+1}{2(\gamma-1)}}}{M_7} = \frac{A}{A^*} \frac{\left(M^{*2} + \frac{2}{\gamma-1}\right)^{\frac{\gamma+1}{2(\gamma-1)}}}{M^*} \tag{9}$$

Here A/A* is the full area ratio, and, since flow through the nozzle is assumed to be a maximum for the approach condition, $M^* = u^*/a^* = 1$. The supersonic value, $M_7 > 1$, is also computed for later use.

Up to this point, the calculation has been straightforward -- no iterations -- for a given incident Mach number (or incident overpressure $(p_2/p_1 - 1) \cdot p_1$) and a given area ratio, A/A*.

Expansion

We replace the actual unsteady expansion process by a steady, quasi-one-dimensional expansion in a hypothetical divergent nozzle. Two cases must be considered for a given A/A*: 1) recompression of the expanded gases is required within the divergent nozzle, and 2) recompression is required after expansion to the full tube area has taken place.

When expansion to the full tube area takes place, we have the situation depicted in Figure 2d, M_7 equals the value computed from Equation (9), and we proceed with the following equations for steady isentropic expansion:

$$\frac{a_7}{a_1} = \frac{a_{6'}}{a_1} \left\{ \frac{M_{6'}^2 + \frac{2}{\gamma-1}}{M_7^2 + \frac{2}{\gamma-1}} \right\}^{1/2} \tag{10}$$

$$\frac{u_7}{a_1} = M_7 \cdot \frac{a_7}{a_1} \tag{11}$$

$$\frac{p_7}{p_1} = \frac{p_7}{p_6} \cdot \frac{p_6}{p_1} = \left\{ \frac{a_7/a_1}{a_6/a_1} \right\}^{\frac{2\gamma}{\gamma-1}} \cdot \frac{p_6}{p_1} \tag{12}$$

Across the recompression or inward-facing shock, which moves to the right behind the transmitted shock wave with a Mach number M_c, we compute:

$$\frac{p_8}{p_7} = \frac{2\gamma}{\gamma+1} M_c^2 - \frac{\gamma-1}{\gamma+1}; \qquad \frac{p_8}{p_1} = \frac{p_8}{p_7} \cdot \frac{p_7}{p_1} \tag{13}$$

and

$$\frac{u_8}{a_7} = M_7 - \frac{2}{\gamma+1} \left(M_c - \frac{1}{M_c}\right); \qquad \frac{u_8}{a_1} = \frac{u_8}{a_7} \cdot \frac{a_7}{a_1} \tag{14}$$

Across the transmitted shock wave:

$$\frac{p_9}{p_1} = \frac{2}{\gamma+1} M_{S_T}^2 - \frac{\gamma-1}{\gamma+1} \tag{15}$$

and

$$\frac{u_9}{a_1} = \frac{2}{\gamma+1} \left(M_{S_T} - \frac{1}{M_{S_T}}\right) \tag{16}$$

The solution is obtained by Newton iteration procedure to find an M_c for which the equations $p_8/p_1 = p_9/p_1$ and $u_8/a_1 = u_9/a_1$ are matched across the contact front. Or, the equations can be solved graphically.

Solutions are valid for a given A/A* so long as $M_c < M_7$. Solutions can also be found for $M_c > M_7$, but this requires that u_7 be negative. This unrealistic result occurs for low incident overpressures.

The limiting value of incident overpressure which satisfies the set of equations above is found for a given A/A* when $M_c = M_7$, where M_7 is the value computed from Equation (9). That is, the limit is found when the inward-facing shock stands at the nozzle exit. For incident overpressures less than this limiting value (for a given A/A*) the inward-facing shock stands in the divergent nozzle as shown in Figure A1.

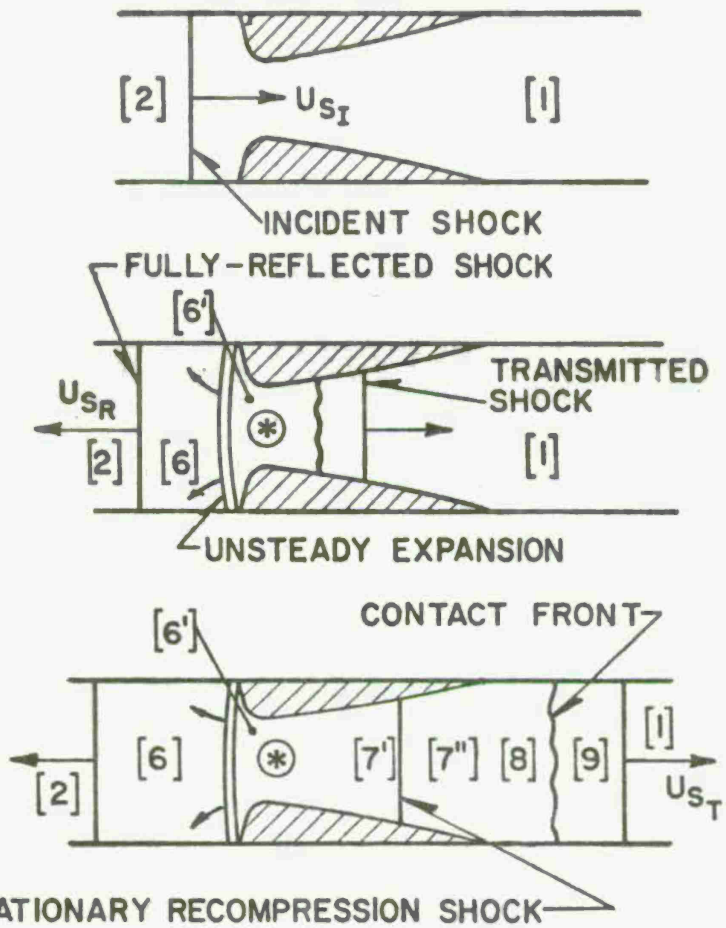

Figure A1. Sketch of Flow Model: Model 4 with Recompression Shock Standing in the Divergent Nozzle.

For this case, we seek a solution for which $M_{7'} \leq M_7$ and $A_{7'}/A^* = A_7''/A^* \leq A/A^*$ using the following equations:

For steady, isentropic expansion to $A_{7'}/A^*$ in the divergent nozzle:

$$\frac{A_{7'}}{A^*} = \frac{\left(M_{7'}^2 + \frac{2}{\gamma-1}\right)^{\frac{\gamma+1}{2(\gamma-1)}}}{M_{7'}} \cdot \frac{M^*}{\left(M^{*2} + \frac{2}{\gamma-1}\right)^{\frac{\gamma+1}{2(\gamma-1)}}} \leq \frac{A}{A^*} \qquad (9)'$$

and

$$\frac{a_{7'}}{a_1} = \frac{a_{6'}}{a_1} \left\{ \frac{M_{6'}^2 + \frac{2}{\gamma-1}}{M_{7'}^2 + \frac{2}{\gamma-1}} \right\}^{1/2} \qquad (10)'$$

$$\frac{u_{7'}}{a_1} = M_{7'} \cdot \frac{a_{7'}}{a_1} \qquad (11)'$$

$$\frac{p_{7'}}{p_1} = \frac{p_{7'}}{p_6} \cdot \frac{p_6}{p_1} = \left\{ \frac{a_{7'}/a_1}{a_6/a_1} \right\}^{\frac{2\gamma}{\gamma-1}} \cdot \frac{p_6}{p_1} \qquad (12)'$$

Across the stationary shock, $M_c = M_{7'}$ and:

$$Y_c \equiv \frac{p_{7''}}{p_{7'}} = \frac{2\gamma}{\gamma+1} M_c^2 - \frac{\gamma-1}{\gamma+1} ; \quad \frac{p_{7''}}{p_1} = Y_c \cdot \frac{p_{7'}}{p_1} \qquad (13)'$$

$$\frac{a_{7''}}{a_{7'}} = \left\{ \frac{Y_c\left(Y_c + \frac{\gamma+1}{\gamma-1}\right)}{\frac{\gamma+1}{\gamma-1} Y_c + 1} \right\}^{1/2}; \quad \frac{a_{7''}}{a_1} = \frac{a_{7''}}{a_{7'}} \cdot \frac{a_{7'}}{a_1} \qquad (14)'$$

$$\frac{u_{7''}}{a_1} = M_{7'} - \frac{2}{\gamma+1}\left(M_c - \frac{1}{M_c}\right) \quad ; \quad \frac{u_{7''}}{a_1} = \frac{u_{7''}}{a_{7'}} \cdot \frac{a_{7'}}{a_1} \qquad (15)'$$

$$M_{7''} = \frac{u_{7''}/a_{7'}}{a_{7''}/a_{7'}} \qquad (16)'$$

For steady, isentropic nozzle expansion to state [8]:

$$\frac{\left(M_8^2 + \frac{2}{\gamma-1}\right)^{\frac{\gamma+1}{2(\gamma-1)}}}{M_8} = \frac{A}{A^*} \cdot \frac{A^*}{A_{7'}} \cdot \frac{\left(M_{7''}^2 + \frac{2}{\gamma-1}\right)^{\frac{\gamma+1}{2(\gamma-1)}}}{M_{7''}} \qquad (17)'$$

and

$$\frac{a_8}{a_1} = \frac{a_{7''}}{a_1} \left\{ \frac{M_{7''}^2 + \frac{2}{\gamma-1}}{M_8^2 + \frac{2}{\gamma-1}} \right\}^{1/2} \qquad (18)'$$

$$\frac{u_8}{a_1} = M_8 \cdot \frac{a_8}{a_1} \qquad (19)'$$

$$\frac{p_8}{p_1} = \frac{p_8}{p_{7''}} \cdot \frac{p_{7''}}{p_1} = \left\{ \frac{a_8/a_1}{a_{7''}/a_1} \right\}^{\frac{2\gamma}{\gamma-1}} \cdot \frac{p_{7''}}{p_1} \qquad (20)'$$

Equations (15) and (16) are again used to compute the conditions behind the transmitted shock wave. Again, we seek a value of M_c (= $M_{7'}$) for which the equations $p_8/p_1 = p_9/p_1$ and $u_8/a_1 = u_9/a_1$ are matched across the contact front. Newton iteration did not work well for this latter set of equations, so the "half-interval method" was used.

LIST OF SYMBOLS

A	cross-sectional area of the tube
a	local gas sound velocity
A^*	sum of the cross-sectional areas of the holes in the plate
M	local Mach number of gas
$M^* = u^*/a^*$	
$= 1$	Mach number of gas at sonic conditions
$M_s \equiv U_s/a$	Mach number of shock wave
p	pressure
U_s	velocity of shock wave
u	local gas velocity
Y	pressure ratio across shock wave
γ	ratio of specific heats, adiabatic exponent
ρ	density

Subscripts

1,2,---	regions indicated on Figure 2
c	pertains to inward-facing shock
I	pertains to incident shock wave
R	pertains to reflected shock wave
T	pertains to transmitted shock wave

DISTRIBUTION LIST

No. of Copies	Organization
12	Commander Defense Documentation Center ATTN: DDC-TCA Cameron Station Alexandria, Virginia 22314
1	Director Defense Advanced Research Projects Agency 1400 Wilson Boulevard Arlington, Virginia 22209
1	Director Weapons Systems Evaluation Group ATTN: CPT Donald E. McCoy Washington, DC 20305
3	Director Institute for Defense Analyses ATTN: Dr. J. Menkes Dr. J. Bengston Tech Info Ofc 400 Army-Navy Drive Arlington, Virginia 22202
1	Assistant to the Secretary of Defense (Atomic Energy) ATTN: Document Control Washington, DC 20301
1	Office Secretary of Defense Office DDR&E ATTN: Mr. J. Persh, Staff Specialist Materials and Structures Washington, DC 20301
2	Chairman Joint Chiefs of Staff ATTN: J-3, Operations J-5, Plans & Policy (R&D Division) Washington, DC 20301
2	Director Defense Nuclear Agency ATTN: Mr. J. F. Moulton, SPAS Dr. E. Sevin, SPSS Washington, DC 20305
4	Director Defense Nuclear Agency ATTN: SPTL Tech Lib (2 cys) APSI (ARCHIVES) STSP Washington, DC 20305
1	Commander Field Command Defense Nuclear Agency ATTN: Tech Lib, FCWS-SC Kirtland AFB New Mexico 87115
1	Chief Las Vegas Liaison Office Field Command TD, DNA P.O. Box 2702 ATTN: Document Control Las Vegas, Nevada 89104
1	DNA Information and Analysis Center TEMPO, General Electric Co. Center for Advanced Studies ATTN: DASIAC 816 State Street Santa Barbara, California 93102
1	Director Defense Communications Agency ATTN: NMCSSC (Code 510) Washington, DC 20305
2	Director Defense Intelligence Agency ATTN: DT-1C, Dr. J. Vorona DT-2 Washington, DC 20301

DISTRIBUTION LIST

No. of Copies	Organization
1	Commander US Army Materiel Development and Readiness Command ATTN: DRCDMA-ST 5001 Eisenhower Avenue Alexandria, VA 22333
1	Commander US Army Materiel Development and Readiness Command ATTN: DRCPM-CS 5001 Eisenhower Avenue Alexandria, VA 22333
1	Commander US Army Aviation Systems Command ATTN: DRSAV-E 12th and Spruce Streets St. Louis, MO 63166
1	Director US Army Air Mobility Research and Development Laboratory Ames Research Center Moffett Field, CA 94035
1	Commander US Army Electronics Command ATTN: DRSEL-RD Fort Monmouth, NJ 07703
3	Commander US Army Missile Command ATTN: DRSMI-R DRSMI-AOM, Lib DRSMI-RSS, Mr. B. Cobb Redstone ARsenal, AL 35809
2	Commander US Army Missile Command ATTN: DRSMI-RX, W. Thomas DRSMI-RR, L. Lively Redstone Arsenal, AL 35809
2	Commander US Army Tank Automotive Development Command ATTN: DRDTA DRDTA-RWL Warren, MI 48090
2	Commander US Army Mobility Equipment Reearch & Development Command ATTN: Tech Docu Cen, Bldg. 315 DRSME-RZT Fort Belvoir, VA 22060
3	Commander US Army Armament Command ATTN: DRSAR-RDT DRSAR-RDN DRSAR-MT Rock Island, IL 61202
3	Commander US Army Armament Command ATTN: DRSAR-SC, Dr. C. Hudson DRSAR-SF, R. Young DRSAR-PPI, CPT Burnsteel Rock Island, IL 61202
3	Commander US Army Armament Command ATTN: Joint Army-Navy-Air Force Conventional Ammunition Prod Coord Gp/E. Jordan Rock Island, IL 61202
1	Commander US Army Frankford Arsenal ATTN: SARFA-L6100, Dr. P. Flynn Philadelphia, PA 19137
1	Commander US Army Rock Island Arsenal Rock Island, IL 61202

DISTRIBUTION LIST

No. of Copies	Organization
4	Commander US Army Picatinny Arsenal ATTN: SARPA-V Mr. G. Demitrack Mr. M. Weinstein SARPA-MT-F Mr. John Canavan DRCPM-PBM-E, Mr. Dybacki Dover, NJ 07801
1	Commander Dugway Proving Ground ATTN: STEDP-TO-H, Mr. Miller Dugway, UT 84022
1	Commander US Army Watervliet Arsenal Watervliet, NY 12189
1	Commander Pine Bluff Arsenal Pine Bluff, AR 71601
1	Commander Cornhusker Army Ammunition Plant Grand Island, NE 68801
1	Commander Indiana Army Ammunition Plant Charlestown, IN 47111
1	Commander Iowa Army Ammunition Plant Burlington, IA 52502
1	Commander Joliet Army Ammunition Plant Joliet, IL 60436
1	Commander Kansas Army Ammunition Plant Parsons, KS 67357
1	Commander Lone Star Army Ammunition Plant Texarkana, TX 75502
1	Commander Longhorn Army Ammunition Plant Marshall, TX 75671
1	Commander Louisiana Army Ammunition Plant Shreveport, LA 71102
1	Commander Milan Army Ammunition Plant Milan, TN 38358
1	Commander Radford Army Ammunition Plant Radford, VA 24141
1	Commander Ravenna Army Ammunition Plant Ravenna, OH 44266
1	Director US Army Engineer School Fort Belvoir, VA 22060
1	Commander US Army Harry Diamond Labs ATTN: DRXDO-TI 2800 Powder Mill Road Adelphi, MD 20783
1	Commander US Army Materials and Mechanics Research Center ATTN: DRXMR-ATL Watertown, MA 02172
1	Commander US Army Natick Research and Development Command ATTN: DRXRE, Dr. D. Sieling Natick, MA 01762

DISTRIBUTION LIST

No. of Copies	Organization
1	Commander US Army Foreign Science and Technology Center ATTN: Rsch & Data Branch Federal Office Building 220 7th Street, NE Charlottesville, VA 22901
1	Director DARCOM Field Safety Activity ATTN: DRXOS-ES Charlestown, IN 47111
1	Director DARCOM, ITC ATTN: Dr. Chiang Red River Depot Texarkana, TX 75501
1	Commander US Army TRADOC Systems Analysis Activity ATTN: ATAA-SA White Sands Missile Range NM 88002
2	HQDA (DAMA-AR; NCL Div) Washington, DC 20310
1	Commander US Army Research Office P. O. Box 12211 Research Triangle Park NC 27709
1	Director US Army Advanced BMD Technology Center ATTN: M. Whitfield Huntsville, AL 35807
1	Commander US Army Ballistic Missile Defense Systems Command ATTN: J. Veeneman P. O. Box 1500, West Station Huntsville, AL 35807
1	HQDA (DAEN-MCE-D, R. Wright) Washington, DC 20314
1	HQDA (DAEN-MCC-D, L. Foley) Washington, DC 20314
1	Director US Army Engineer Waterways Experiment Station P. O. Box 631 Vicksburg, MS 39180
1	Division Engineer US Army Engineer Division Fort Belvoir, VA 22060
1	US Army Engineer Division ATTN: Mr. Char P. O. Box 1600 Huntsville, AL 35809
2	Director Joint Strategic Target Planning Staff ATTN: JLTW JPTP Offutt AFB, NE 68113
4	Chief of Naval Operations ATTN: OP-03EG OP-97 OP-754 OP-985FZ Department of the Navy Washington, DC 20350

DISTRIBUTION LIST

No. of Copies	Organization
1	Assistant Secretary of the Navy (Research & Development) Navy Department Washington, DC 20350
1	Chief of Naval Material Navy Department ATTN: Code 418, Dr. T. Quinn Arlington, Virginia 22217
1	Commander Bureau of Naval Weapons ATTN: Code F121 Mr. H. Roylance Department of the Navy Washington, DC 20360
1	Commander Naval Ordnance Systems Command ATTN: Code ORD 43B Mr. Fernandes Washington, DC 20360
2	Commander David W. Taylor Naval Ship Research and Development Center ATTN: Mr. A. Wilner, Code 1747 Dr. W. W. Murray, Code 17 Bethesda, Maryland 20084
3	Commander U.S. Naval Surface Weapons Center ATTN: Mr. F. Sancher Mr. J. C. Talley Dr. W. Soper Dahlgren, Virginia 22448
3	Commander U.S. Naval Surface Weapons Center ATTN: Dr. Leon Schindel Dr. Victor Dawson Dr. P. Huang Silver Spring, Maryland 20910
2	Commander Naval Surface Weapons Center ATTN: Code 241 (Mr. Proctor) (Mr. Kushner) Silver Spring, Maryland 20910
1	Commander U.S. Naval Weapons Center ATTN: Code 6031 Dr. W. Stronge China Lake, California 93555
1	Commander Naval Ammunition Depot ATTN: ORD-04M/B/X-5/L. Leonard Crane, IN 47522
1	Commander Naval Explosive Ord Disposal Facility ATTN: Code 501/L. Wolfson Indianhead, MD 20640
1	Commander U.S. Naval Ship Research and Development Center Facility ATTN: Mr. Lowell T. Butt Underwater Explosions Research Division Portsmouth, Virginia 23709
1	Commander U.S. Naval Weapons Evaluation Facility ATTN: Document Control Kirtland AFB Albuquerque, New Mexico 87117
1	Commander Naval Civil Engineering Laboratory ATTN: J. Tancreto Port Hueneme, CA 93041
1	Director U.S. Naval Research Laboratory ATTN: Code 2027, Tech Lib Washington, DC 20390

DISTRIBUTION LIST

No. of Copies	Organization
2	Superintendent U.S. Naval Postgraduate School ATTN: Tech Reports Sec. Code 57, Prof. R. Ball Monterey, California 93940
1	HQ USAF (AFNIE-CA) Washington, DC 20330
4	HQ USAF (AFRDQ: AFRDOSM); AFRDPM; AFRD) Washington, DC 20330
1	AFSC (DSCPSL) Andrews AFB Washington, DC 20331
1	HQ AFSC Andrews AFB Washington, DC 20334
1	AFRPL (M. Raleigh) Edwards AFB, CA 93523
2	AFATL (ATRD, R. Brandt) Eglin AFB Florida 32542
1	ADTC (ADBPS-12) Eglin AFB Florida 32542
1	ADTC (DOM/S. Reither) Eglin AFB, FL 35242
1	USAFTAWC (OA) Eglin AFB Florida 32542
1	Commander Hill AFB ATTN: MMNTR/Cummings Clearfield, UT 84406
3	AFWL (WLA; WLD; WLRP, LTC H. C. McClammy) Kirtland AFB New Mexico 87117
1	AFSWC (SWTSX) Kirtland AFB New Mexico 87117
4	AFWL (SYT, MAJ W. A. Whitaker; SRR; WSUL; SR) Kirtland AFB New Mexico 87117
1	Commander AF Civil Engineering Center ATTN: AFCEC-DE/LTC Walkup Tyndall Air Force Base Panama City, FL 32401
2	AFLC (MMWM/CPT D. Rideout; IGYE/K. Shopker) Wright-Patterson AFB, OH 45433
2	AFFDL (FDTR) (Dr. F. J. Janik, Jr. Dr. R. M. Bader) Wright-Patterson AFB Ohio 45433
4	AFML (MAMD, Dr. T. Nicholas; MAS: MANC, Mr. D. Schmidt; MAX, Dr. A. M. Lovelace) Wright-Patterson AFB Ohio 45433
2	FTD (TDPTN: TDFBD, J. D. Pumphrey) Wright-Patterson AFB Ohio 45433
1	Headquarters Energy Research and Development Administration Department of Military Applications Washington, DC 20545

DISTRIBUTION LIST

No. of Copies	Organization
1	Energy Research & Development Administration Deputy Manager of Engineering ATTN: W. H. Jackson P.O. Box E Oak Ridge, TN 37830
1	Director ATTN: J. Nall P.O. Box 1925 Washington, DC 20505
2	Director National Aeronautics and Space Administration Lewis Research Center ATTN: Frank Belles G. Pinkas 21000 Brook Park Road Cleveland, OH 44135
2	National Aeronautics and Space Administration Aerospace Safety Research and Data Institute ATTN: Mr. S. Weiss Mail Stop 6-2 Mr. R. Kemp Mail Stop 6-2 Lewis Research Center Cleveland, Ohio 44135
1	Director National Aeronautics and Space Administration Scientific and Technical Information Facility P.O. Box 8757 Baltimore/Washington International Airport Maryland 21240
1	Director Lawrence Livermore Laboratory Technical Information Division P.O. Box 808 Livermore, California 94550
1	Director Los Alamos Scientific Lab. ATTN: Dr. J. Taylor P.O. Box 1663 Los Alamos, New Mexico 87544
1	National Academy of Sciences ATTN: Mr. D. G. Groves 2101 Constitution Avenue, NW Washington, DC 20418
1	Aeronautical Research Associates of Princeton, Inc. ATTN: Dr. C. Donaldson 50 Washington Road Princeton, New Jersey 08540
1	Aerospace Corporation ATTN: Dr. Harris Mayer P.O. Box 95085 Los Angeles, California 90045
2	AVCO Corporation Structures and Mechanics Dept. ATTN: Dr. William Broding Mr. J. Gilmore Wilmington, Massachusetts 01887
2	The Boeing Company Aerospace Group ATTN: Dr. Peter Grafton Dr. D. Strome Mail Stop 8C-68 Seattle, Washington 98124
1	Dr. J. C. Shang General American Research Div General American Transportation Corp 7449 N. Natchez Avenue Niles, Illinois 60648
1	Hercules, Inc. ATTN: Billings Brown Box 93 Magna, UT 84044

DISTRIBUTION LIST

No. of Copies	Organization
1	J.G. Engineering Research Associates 3831 Menlo Drive Baltimore, MD 21215
2	Kaman-Avidyne ATTN: Dr. N. P. Hobbs Mr. S. Criscione 83 Second Avenue Northwest Industrial Park Burlington, MA 01803
3	Kaman Sciences Corporation ATTN: Dr. F. H. Shelton Dr. D. Sachs Dr. R. Keefe 1500 Garden of the Gods Road Colorado Springs, CO 80907
1	Knolls Atomic Power Lab ATTN: Dr. R. A. Powell Schenectady, NY 12309
2	Martin Marietta Laboratories ATTN: Dr. P. F. Jordan Mr. R. Goldman 1450 S. Rolling Road Baltimore, MD 21227
1	McDonnell Douglas Astronautics Western Division ATTN: Mr. Samuel D. Mihara 3000 Ocean Park Boulevard Santa Monica, CA 90406
1	Monsanto Research Corporation Mound Laboratory ATTN: Frank Neff Miamisburg, OH 45342
1	Physics International ATTN: Dr. G. Richard Fowles San Leandro, CA 94577
1	R&D Associates ATTN: Mr. John Lewis P. O. Box 9695 Marina del Rey, CA 90291
2	Sandia Laboratories ATTN: Info Distr Division Dr. W.A. Von Riesemann Albuquerque, NM 87115
2	Battelle Columbus Laboratories ATTN: Dr. L. E. Hulbert Mr. J. E. Backofen, Jr. 505 King Avenue Columbus, OH 43201
1	Brown University Division of Engineering ATTN: Prof. R. Clifton Providence, RI 02912
1	Georgia Institute of Tech ATTN: Dr. S. Atluri 225 North Avenue, NW Atlanta, GA 30332
1	Massachusetts Institute of Technology Aeroelastic and Structures Research Laboratory ATTN: Dr. E. A. Witmer Cambridge, MA 02139
1	Ohio State University Department of Engineering Mechanics ATTN: Prof. K. K. Stevens Columbus, OH 43210
3	Southwest Research Institute ATTN: Dr. H. N. Abramson Dr. W. E. Baker Dr. U. S. Lindholm 8500 Culebra Road San Antonio, TX 78228

DISTRIBUTION LIST

No. of Copies	Organization
1	Stanford Research Institute ATTN: Dr. W. Reuland 306 Wynn Drive, NW Huntsville, AL 35805
1	Texas A&M University Department of Aerospace Engineering ATTN: Dr. James A. Stricklin College Station, TX 77843
1	University of Alabama ATTN: Dr. T. L. Cost P. O. Box 2908 University, AL 35486
1	University of Delaware Department of Mechanical and Aerospace Engineering ATTN: Prof. J. R. Vinson Newark, DE 19711

No. of Copies	Organization
	Aberdeen Proving Ground
	Marine Corps Ln Ofc
	Dir, USAMSAA ATTN: Dr. J. Sperrazza Mr. R. Norman, WSD
	Cdr, APG ATTN: STEAP-AD-R/RHA
	Cdr, USAEA ATTN: SAREA-MT-T Mr. R. Thresher Dr. D. Katsanis Mr. B. Jezek Mr. J. McKivrigan